Discovery of BMS-986408, a First-In-Class Dual DGKα and DGKζ Inhibitor That Unleashes PD-1 Checkpoint and CAR T-Cell Immunotherapies

Michael Wichroski[1*,#], Si-Qi Liu[1,#], Lauren M Zasadil[5], Joseph L. Benci[2], Patrick C. Gedeon[7], Kendall J. Condon[2], Suhasini Joshi[4], Shana Posy[2], Patrick Carlson[3], Alison Maier[3], Jiao Shen[6], Rakeeb Kureshi[6], Yuka Amako[1], Tai Wang[1], Ryan L. Powles[1], Yanyun Li[2], Tho Lai[2], Igor Katsyv[1], Hongchen Qiu[1], Huilin Qi[1], Jessica Wong[1], Dandan Zhao[2], Dana Banas[2], Joelle Onorato[2], Gregory Locke[2], Xueer Chen[1], Wen-Chi Chou[1], Erica Cook[1], Abigail E. Witt[1], Christopher M. Barbieri[2], Hong Zhang[1], Jonathan B. Olsen[2], Alba Font Tello[1], Eugene Drokhlyansky[1], Denise C. Grünenfelder[1], Louis Chupak[1], Tyler A. Longmire[1], Jon C. Jones[3], Travis J. Hollmann[2], David G. Kugler[3], John N. Feder[2], Raphael Bueno[7], John Wain[7], Pallavur Sivakumar[3], Yu Liu[1], Stephanie K. Dougan[6], Cloud P. Paweletz[5], David A. Barbie[5], and Emma Lees[1]

[1]Research and Development, Bristol Myers Squibb Company, Cambridge, MA, USA.

[2]Research and Development, Bristol Myers Squibb Company, Lawrenceville, NJ, USA.

[3]Research and Development, Bristol Myers Squibb Company, Seattle, WA, USA.

[4]Research and Development, Bristol Myers Squibb Company, San Diego, CA, USA

[5]Department of Medical Oncology, Dana-Farber Cancer Institute, Boston, MA, USA.

[6]Department of Cancer Immunology and Virology, Dana-Farber Cancer Institute and Harvard Medical School, Boston, MA, USA.

[7]Department of Surgery, Brigham and Women's Hospital and Harvard Medical School, Boston, MA, USA.

*Corresponding author. Email: michael.wichroski@gmail.com

[#]These authors contributed equally: Michael Wichroski, Si-Qi Liu

Keywords: Diacylglycerol kinase, DGKα, DGKζ, immunotherapy, PD-1, CAR-T cell, NSCLC, PDOTs

Authors' Disclosures: All authors declare that they have no conflicts of interest to disclose.

Funding Information: All studies were funded by Bristol Myers Squibb.

Running Title: Discovery of first-in-class dual DGKα/ζ inhibitor BMS-986408

Abstract

Diacylglycerol kinase α (DGKα) and DGKζ are lipid kinases that negatively regulate T-cell signaling through diacylglycerol (DAG) metabolism, making them attractive targets for next-generation immunotherapy. Here, we report the discovery and pre-clinical characterization of the clinical-stage DGKα and DGKζ lipid kinase inhibitor, BMS-986408. BMS-986408 binds to the accessory subdomain of the catalytic domain and inhibits DGKα/ζ through a mechanism of action that includes competitive inhibition for the DAG substrate, subcellular translocation to the plasma membrane, and proteosome-dependent degradation. DGKα/ζ inhibition markedly improved the therapeutic benefit of PD-1 therapy by unleashing T-cell responses in the tumor while also amplifying the priming and expansion of tumor-reactive T cells in the tumor-draining lymph nodes. Simultaneous inhibition of both DGKα and DGKζ was required to maximize combination benefit with PD-1 therapy. Further, we observed in non-small cell lung cancer (NSCLC) patient samples that DGKα and DGKζ were broadly expressed in tumor-infiltrated T cells and combination therapy invigorated a robust cytokine response in NSCLC patient–derived organotypic tumors supporting the clinical evaluation of this combination in NSCLC patients. BMS-986408 also markedly improved CD19-targeted CAR T-cell therapy efficacy by overcoming hypo-functionality, insufficient expansion, and lack of co-stimulatory ligands. BMS-986408 represents a critical step toward evaluating the broad immunotherapy potential of DGKα/ζ inhibitors in cancer patients.

Synopsis

DGKα and DGKζ negatively regulate T-cell signaling. The authors show that BMS-986408, a first-in-class dual DGKα/ζ inhibitor, potentiates T cell–receptor signaling and T-cell activation, enhancing the effectiveness of both PD-1 and CAR T-cell therapy in preclinical models.

Introduction

Immunotherapies are revolutionizing cancer patient treatment. Innovations in T-cell checkpoint inhibitors (e.g., PD-1, PD-L1, and CTLA-4 therapeutic antibodies), chimeric antigen receptor (CAR) T cells, adoptive T-cell transfer and bispecific T-cell engagers have improved patient survival across a broad range of indications (1). However, challenges remain, and next-generation therapeutic strategies that improve T-cell functionality are needed to overcome both primary and acquired resistance (2).

As a central negative regulatory node in T-cell receptor (TCR) signaling, inhibiting T-cell diacylglycerol (DAG) metabolism has emerged as a high priority drug discovery strategy, which has the potential to improve both PD-1 immune checkpoint inhibitor therapy (3-5) and CAR T-cell therapy (6). In T cells, the diacylglycerol kinase α (DGKα) and DGKζ lipid kinases convert the TCR-induced secondary messenger DAG into phosphatidic acid (PA), which detunes downstream signaling through the Ras-ERK, PKC, and NF-κB pathways that are required for T-cell activation (7). Together, DGKα and DGKζ operate as an intracellular T-cell checkpoint, suppressing TCR signaling and promoting both T-cell anergy and exhaustion (7-9). In the context of T-cell anergy, DGKα and DGKζ contribute to functional unresponsiveness in T cells that have been exposed to antigen without proper co-stimulation, thereby preventing inappropriate immune responses (10). While important for maintaining immune homeostasis and preventing autoimmunity, DGKα and DGKζ limit T cell–mediated tumor immunity, especially in the context of low-affinity antigen presentation, insufficient co-stimulation, and low major histocompatibility complex class I expression on tumor cells (3,4). Genetic studies in T cells and CAR T-cell models have shown that DGKα and DGKζ synergistically regulate T-cell activation

and effector functions (5,6,9,11), suggesting that targeting both DGKα and DGKζ will be critical to capture the various contexts relevant to T cell–mediated tumor immunity.

Recently, we presented the important first step towards delivering a dual DGKα/ζ inhibitor to the clinic with the discovery of a first-in-class chemical series that selectively inhibited both DGKα and DGKζ through an unknown binding site (3,12). This was achieved using an innovative T-cell phenotypic screening approach coupled with chemical proteomics for target identification (3,12). Here, we present the next chapter of our drug discovery journey with the discovery and characterization of the clinical-stage DGKα/ζ inhibitor BMS-986408. We describe the complex BMS-986408 mechanism of action, including binding site identification using a CRISPR base editing approach, DAG substrate competitive lipid kinase inhibition, subcellular translocation to plasma membrane, and proteosome-mediated degradation. Through preclinical studies, we showed that DGKα/ζ inhibition markedly improved the therapeutic benefit of PD-1 therapy by unleashing T-cell effector responses in tumors and amplifying the priming and expansion of tumor-reactive T cells in lymph nodes. In support of a dual DGKα/ζ inhibitor strategy in the clinic, we show that inhibiting both DGKα and DGKζ isozymes was required to maximally potentiate TCR signaling, T-cell activation, and therapeutic benefit in combination with PD-1 therapy. Through translational research studies, we have provided strong rationale for the clinical combination of BMS-986408 and PD-1 therapy in non-small cell lung cancer (NSCLC). Finally, we showed that dual DGKα/ζ inhibition invigorated CAR T-cell therapeutic efficacy by addressing many of the hallmarks of poor CAR T-cell therapy response including hypofunctionality induced by chronic stimulation, poor expansion and low tumor co-stimulation. These studies highlight the broad immunotherapy potential of BMS-986408 and support its clinical evaluation in combination with both PD-1 and CAR T-cell therapies.

Materials and Methods

Compounds

BMS-986408 synthesis was described in patents WO 041588 and US 0061802, 2021 (example 5/6), DGKα-i synthesis was described in patent WO 105115, 2021 (example 48) and DGKζ-i was synthesized using procedures analogous to example 293 in US 0061802, 2021, employing 5-bromo-1-methyl-3-(trifluoromethyl)-1H-1,2,4-triazole and 3-(trifluoromethyl)benzaldehyde.

Animals

C57BL/6 (IMSR_JAX:000664), Balb/c (IMSR_JAX:000651), OT1 (IMSR_JAX:003831), Nur77-GFP reporter (IMSR_JAX:016617) and NSG (IMSR_JAX:005557) mice were acquired from The Jackson Laboratory. $TRP1^{High}Rag2^{-/-}$ and $TRP1^{Low}Rag2^{-/-}$ mice were maintained in Dana Faber Cancer Institute (DFCI). All in vivo studies protocols were approved by Bristol Myers Squibb Institutional Animal Care and Use Committee (IACUC) and DCFI IACUC. All animal studies in the CAR T section were conducted by Bristol Myers Squibb (Seattle, WA), with animals housed at Omeros Corporation (Seattle, WA), in strict accordance with Omeros's Institutional Animal Care and Use Committee protocol IR# 21-02.

Cell lines

Jurkat cells (CVCL_0065) was acquired from American Type Culture Collection (ATCC). DGKα-YFP and DGKζ-YFP Jurkat cells was generated by transducing the Jurkat cells with lentivirus harboring DGKA-YFP and DGKZ-YFP coding sequences (Supplementary Table S1). Jurkat cells with or without engineering were maintained in Roswell Park Memorial Institute (RPMI; ThermoFisher) with 10% heat-inactivated Fetal Bovine Serum (HI-FBS; ThermoFisher). HEK293A cells was acquired from Promega. HEK293A cells were transfected with DGKα-

NanoLuc (Promega, Catalog# CS1810C483) or NanoLuc-DGKζ (Promega, Catalog# CS1810C489) constructs with FuGENE® HD kit (Promega) according to manufacturer's instructions. HEK293A cells with or without engineering were maintained in Dulbecco's Modified Eagle Medium (DMEM; ThermoFisher) with 10% HI-FBS. SAOS-2 cells (CVCL_0548) were acquired from ATCC and maintained in McCoy 5A medium (ThermoFisher) with 10% HI-FBS. SOAS-2-GFP/Luc cells were generated by transducing SOAS-2 cells with lentivirus harboring GFP/Luciferase coding sequence (System Biosciences, Catalog# BLIV101PA-1).

Raji (CCL-86), K562 (CCL-243), and A549 (CCL-185) cells were acquired from American Type Culture Collection (ATCC) between 2015 and 2017. Nalm6 (ACC-128), Granta-519 (ACC-342) cells were acquired from the Leibniz Institute DSMZ in 2015. Versions of K562 and A549 expressing the CD19 antigen (K562-CD19 and A549-CD19) were generated by transducing K562 cells or A549 cells with a lentivirus vector containing the coding sequence for human CD19. CD19+ K562 and CD19+ A549 cells were sorted for purity by flow cytometry. K562-CD19 and A549-CD19 cells were then transduced with a separate lentivirus vector containing NucLight Red (Sartorius Corporation, #4476). Versions of Raji and Nalm6 cell lines expressing luciferase were generated by transducing parental Raji or Nalm6 cells with RediFect Red-Fluc Lentivirus containing GFP (Perkin Elmer, Catalog# CLS960003). Cells were sorted for GFP^+ expression. Granta-519, K562-CD19, Nalm6, Raji, and A549-CD19 cells were maintained in RPMI media supplemented with 10% HI-FBS. Luciferase expressing Raji and Nalm6 cells were grown in RPMI media supplemented with 10% HI-FBS, non-essential amino acids (NEAA), Sodium Pyruvate, and 1:1000 β-Mercaptoethanol. All media components were purchased from ThermoFisher.

Mouse tumor cell lines, MC38, CT26 (CVCL_7254), and SA1N (CVCL_6443) were utilized for the in vivo study. The MC38 cell line was kindly gifted by Dr. James Allison (MD Anderson Cancer Center, University of Texas). CT26 and SA1N cell lines were acquired from ATCC. The MC38 cell line was maintained in DMEM with 10% HI-FBS. CT26 cells were maintained in DMEM with 10% FBS. SA1N cell line was maintained. C2VTrp1 tumor cell line was generated in DFCI as previously described (4). C2VTrp1 was cultured in RPMI with 10% HI-FBS, NEAA, Sodium Pyruvate, GlutaMAX, and Pen/Strep. All components were purchased from ThermoFisher.

All cell lines tested negative for mycoplasma (IDEXX BioAnalytics). All human cell lines were authenticated using short tandem repeat (STR) method in the past year by submitting a cryo preserved vial of cells to LabCorp. Once results were obtained, they were checked against reference sequence in a publicly available database (Cellosaurus).

DGK Knock-in Cell Line Generation

Mutation knock-in cell lines were generated using Cas9:sgRNA ribonuclear proteins (RNPs) with Homology-directed repair (HDR) donor templates delivered by Nucleofection (Lonza). The sequences of sgRNAs and donor ssDNAs are provided in Supplementary Table S1. For nucleofection, 4×10^5 cells in 20 µL solution SE with 40 pmol Cas9 (Alt-R™ S.p. HiFi Cas9 Nuclease V3, IDT) complexed with 200 pmol sgRNA (IDT) and 200 pmol ssODN donor oligos (IDT) were nucleofected with program CL-120. Cells were plated in media containing 10 µM DNA-PK inhibitor M3814 (MedChemExpress) for 24 hours. Single cell cloning was performed by limiting dilution. Sequencing libraries were prepared using the Illumina DNA Prep Kit according to the manufacturer's recommendations and MiSeq run parameters were set at 150bp paired-end, dual indexed using a 300v2 micro reagent kit (Illumina). Samples were

demultiplexed using bcl2fastq v2.2.0, and analyzed with the CRISPR-DAV analysis pipeline as previously described (13). HiBiT KI cell lines were made as above with additional screening by NanoGlo HiBiT detection assay (Promega) prior to next-generation sequencing (NGS). Jurkat-eGFP-DGKα and mNeonGreen-DGKζ reporter cell lines were made as above except that the HDR donor templates were supplied as 1μg long ssDNA (eGFP-DGKA KI HDR donor from IDT, mNeonGreen-DGKZ HDR Donor from Moligo; Solna, Sweden).

Biochemical and cellular DGK lipid kinase assays

DGK family biochemical lipid kinase inhibition was evaluated at Reaction Biology (Malvern, PA) who developed biochemical assays for all 10 DGK isozymes. Their assay platform measured the enzymatic transfer of a phosphate group from ATP to the lipid substrate resulting in phosphorylated substrate and ADP. For the cellular DAG to PA conversion assay, Jurkat cells were washed twice with RPMI then resuspended in RPMI at concentration of 1×10^6 cells/mL. 1 mL cells were plated into a deep 96-well plate. BMS-986408 was added to the cells for 30 minutes. DAG and PA were produced by and purchased from Avanti Polar Lipids (Alabaster, AL). D4-dioleoyl-DAG (5 μL, final concentration 0.5 mM) was then added, and the cells were incubated for 10 minutes, then centrifuged at 1,500 RPM to collect pellets. The supernatant was discarded, and the cell pellets were frozen at -80°C until analysis by liquid chromatography with tandem mass spectrometry (LC-MS/MS). The dried wells containing Jurkat cells were reconstituted in 50 μL of PBS and vortex mixed. The samples (30 μL) were then transferred to a 96-well plate, diluted with 270 μL of internal standard solution (in 0.1% formic acid in methanol), vortex mixed for 10 minutes, then centrifuged. The supernatants (100 μL) were then transferred to a shallow 96-well plate and capped for LC-MS/MS analysis. Calibration standards were treated the same way as samples. The PA product was measured by LC-MS/MS using a

Sciex API5500 mass spectrometer coupled to a Shimadzu Nexera uHPLC pump with autosampler. LC was performed on a Waters BEH C8 50 × 2.1 mm (3.5 µm particle size) column using a column temperature of 65°C, a mobile phase consisting of solvent A = 5 mM ammonium formate in water/methanol/isopropyl alcohol (90:5:5, v/v/v) with 0.2% formic acid and solvent B = 5 mM ammonium formate in isopropyl alcohol/methanol (80:20, v/v) with 0.2% formic acid at a flow rate of 0.5 mL/minute. The LC gradient used was as follows: hold 80% to 100% solvent B for 0.2 minutes, 20% to 80% B in 3.3 minutes, 100% B in 0.1 minutes, hold 100% B for 1 minute. Products were monitored using selected reaction monitoring (SRM) in negative ionization mode. The following ions were monitored: d4-dioleoyl-PA (product) m/z 703.5/283.3, dioleoyl-PA (calibration standard) m/z 699.5/281.5, d7-C15:0-C18:1-PA (internal standard) m/z 666.5/241.2. For quantitation of product, dioleoyl-PA calibration curves were generated in methanol using d7-C15:0-C18:1-PA as an IS; the typical calibration range was 5 ng/mL to 5,000 ng/mL. Data processing was through Analyst software (Sciex).

PhosphoSens Diacylglycerol Phosphorylation Lipid Kinase Assay

A recombinant DGKα (SignalChem, D21-10BH) DAG phosphorylation assay was established using the PhosphoSens kinase assay platform (AssayQuant). Reaction conditions for the DGKα assay were as follows: 53.2 mM HEPES, pH 7.6, 0.5 mM ATP, 1.16 mM DTT, 0.8% glycerol, 0.16 mg/ml bovine serum albumin (BSA), 0.032 mM EDTA, 3 mM $MgCl_2$, 0.4 mM $CaCl_2$, 20 µM SOX, 75 mM NaCl, 180 µM DAG (18:1 1-2-dioleoyl-sn-glycerol, Avanti, 80811), 120 µM 1,2-dioleoyl-sn-glycero-3-phospho-L-serine (Avanti Cat# 840035P), phosphatidyl serine (Sigma), 0.1% TX-100, 0.2% DMSO, and 8 nM of recombinant DGKα. BMS-986408 was serially diluted in 5% DMSO, and the final concentrations in reaction mixture were 10 µM; 3.33 µM; 1 µM; 333 nM; 100 nM; 33.3 nM; 10 nM; 3.33 nM; 1 nM; 333 pM; 100 pM. Enzymes were

diluted in enzyme dilution buffer (EDB) consisting of 20 mM HEPES, pH 7.6, 5% Glycerol, 0.2 mM EDTA, 1 mM DTT, and 1 mg/mL BSA. Reactions were run in half-area 96-well, white flat round bottom polystyrene NBS microplates (Corning, Catalog# 3642) after sealing using optically-clear adhesive film (TopSealA-Plus plate seal, PerkinElmer, applied with a roller) to eliminate evaporation and resulting drift. The reaction set up included adding 5 µL of substrate (1.8 mM DAG plus 1.2 mM PA in 1% TX-100), 2 µL of a 25x stock of BMS-986408 and 35 µL of a 1.43x stock of the reaction mixture (1.43×). The components were incubated for 45 min at 30°C followed by addition of 8 µl of a 6.5x stock of recombinant DGKα. The reaction was run at 30°C for 120 min. To evaluate DAG competition with BMS-986408, the same assay protocol was followed for the DGKα assay with the exception that DAG was tested at ascending concentrations (80, 100, 120, 160, 180, 200, 220, 250 and 300 µM). Reaction velocity versus substrate plots were generated in GraphPad Prism 8.0 and analyzed according to the standard equation for mixed model inhibition:

$$v = \frac{V_{max} \times S}{K_M \left(1 + {}^{I}/_{K_I}\right) + S\left(1 + {}^{I}/_{\alpha K_I}\right)}$$

v is the reaction velocity

Vmax is the maximal reaction velocity

S is the substrate

K_M is the Michaelis-Menten constant

I is the inhibitor

K_I is the inhibition constant

α is the cooperativity equilibrium constant (used to classify the mode of inhibition of BMS-986408 relative to each substrate).

High-content imaging DGK translocation assay

Jurkat cells with DGKα-YFP or DGKζ-YFP were plated into 384-well plates in 40 µL assay media (RPMI with 10% HI-FBS) at 30,000 cells/well and 40 nL of compound was transferred to each well using an ECHO liquid handler (Beckman Coulter) followed by a 1h incubation at 37°C. Cells were fixed by adding 40 µL of 4% formaldehyde diluted in PBS followed by incubation for 15 minutes at room temperature. Plates were centrifuged at 250 RPM for 5 minutes and washed 2× with PBS using an automated washer (BioTek). Cells were blocked by adding 50 µL of 0.3 M Glycine (ThermoFisher) diluted in PBS for 15 minutes at room temperature followed by a single wash with 50 µL PBS. Nuclei were stained using 1:1000 Hoechst diluted in block buffer (ThermoFisher) for 30 minutes at room temperature. Plates were washed 3 times with 50 µL PBS, sealed and centrifuged at 250 RPM for 5 minutes. The cells were imaged using the Opera Phenix (Perkin Elmer) with a 40× water objective. YFP signal was captured and analyzed with the Harmony Software (Revvity), and the membrane translocation was calculated.

Nanoluciferase bioluminescence resonance energy transfer (NanoBRET) DGK target engagement assay

HEK293A with DGKα-NanoLuc or NanoLuc-DGKζ transfection were seeded in 96-well plates at 1×10^4 cells/well and cultured for 24 hours prior to treatment. DGK tracer was diluted in DMSO to 20× in Tracer Dilution Buffer (Promega) and cold compound was prepared at 10× concentration in Opti-MEM (ThermoFisher). 5 µL of the tracer dilutions was added into each well and plates were mixed for 15 seconds. 10 µL of the cold compound dilutions were plated and mixed for 15 seconds. Plates were incubated at 37°C + 5% CO2 for 2 hours followed by NanoBRET Assay. Immediately prior to BRET measurements, a 1:166 dilution (3× solution) of

NanoBRET Nano-glo® Live Cell Solution (Promega), was prepared in Opti-MEM without serum or phenol red and with a 1:500 dilution of Extracellular NanoLuc® Inhibitor (Promega). Plates were removed from the incubator for 15 minutes to reach room temperature. 50 µL per well of 3× NanoBRET Nano-glo® Live Cell Solution was added to each well, incubated for 2-3 minutes, and then donor emission (e.g. 450 nm) and acceptor emission (e.g. 610 nm or 630 nm) were measured using Infinite® 200 PRO plate reader (TECAN). Raw BRET ratio values were calculated by dividing the acceptor emission value (e.g. 610 nm) by the donor emission value (e.g. 450 nm) for each sample and subtracting the BRET ratio in the absence of tracer (average of no tracer control samples) from the BRET ratio of each sample. Raw BRET units were converted to milliBRET units (mBU) by multiplying each raw BRET value by 1000. NanoBRET signal was calculated as:

$$\left(\frac{Acceptor_{sample}}{Donor_{sample}} - \frac{Acceptor_{no\ tracer\ control}}{Donor_{no\ tracer\ control}}\right) \times 1000$$

DGK CRISPR Base Editing and Modeling

For adenine base editing, single-guide RNA (sgRNA) libraries targeting *DGKA* (NM_001345.5) and *DGKZ* (NM_001199267.2) were designed and cloned into pRDA_429 (Addgene plasmid #179098), as previously described by the Broad Institute Genetic Perturbation Platform (GPP) (14), yielding clone pools CP1871 and CP1866. Lentivirus for the DGKA/CP1871 and DGKZ/CP1866 libraries was generated by the GPP and Flash Therapeutics, respectively. Prior to screening, lentiviral titer from both sources was measured in Jurkat-eGFP-DGKα or mNeonGreen-DGKζ reporter cell lines by measuring cell counts after 1µg/mL puromycin selection (ThermoFisher). For infection, 15×10^6 Jurkat-eGFP-DGKα or mNeonGreen-DGKζ cells were transduced with the respective base editor library at a multiplicity of infection (MOI)

<0.30 by spinning at 931 × g for 1 hour at 37°C in media (RPMI + 10% FBS) supplemented with 4μg/mL polybrene. After overnight incubation, cells were resuspended in fresh media and selected with 1μg/mL puromycin. On day 7 post-transduction, cells were treated overnight with DMSO or 750nM BMS-986408. Subsequently, the control DMSO treated cells were passaged and BMS-986408 treated cells were sorted on a FACSAria™ Fusion (BD), collecting the top 10% $eGFP^+$ or $mNeonGreen^+$ cells. The resulting fraction for each screen was split into two replicates and allowed to recover. After sorted replicates recovered, each was retreated with 750nM BMS-986408 and sorted as described above. As a baseline, previously passaged DMSO treated cells were retreated with DMSO and collected for later genomic DNA isolation. Following a second cell recovery, genomic DNA was isolated from DMSO and replicate treatment arms using a NucleoSpin Blood Midi kit (Machery Nagel, catalog no. 740954.20). Genomic DNA was then further purified with a OneStep PCR Inhibitor Removal kit (Zymo Research, Catalog# D6030) and submitted to the Broad Institute (GPP) for library amplification, sequencing, and processing with PoolQ (https://portals.broadinstitute.org/gpp/public/software/poolq). Output log normalized values for compound treated replicate samples were averaged for analysis. The DMSO treated data were then subtracted from the BMS-986408 data to give the log fold change enrichment for each sgRNA.

The AlphaFold models for DGKα (AF-P23743) and DGKζ (AF-Q13574) were downloaded on July 23, 2021. The models were truncated to residues 372–735 (DGKα) and 277–625 (DGKζ) and prepared for docking with Schrodinger v2023-2 ProteinPrep. An initial three-dimensional conformation of BMS-986408 was generated using OpenEye Omega v2.5.1.4 and subjected to conformational search with Schrodinger MacroModel mixed torsional/low mode sampling with default parameters. Schrodinger Induced Fit Docking was applied to the lowest-energy

conformer to dock the ligand to both receptors with standard parameters. The binding site residues were defined in the input file as DGKα 463, 464, 529, 530, 532, 532, 533, 534, 537, 556, 564, 567, 568, 569, 606, 609, 611, 612, and 668. For DGKζ, the binding site residues were defined as 450, 461, 463, 463, 466, 481, 482, 482, 483, 483, 489, 490, 490, 492, 524, 533, 534, 555, and 569. The top pose was selected for DGKα and the pose most similar to the DGKα pose was selected for DGKζ.

DGK cellular thermal shift assay (CETSA)

CETSA assay was performed according to a previous report (15) and adapted with some customization. Briefly, CRISPR Knock-in (KI) HiBiT tagged *DGKA* and *DGKZ* Jurkat cells were obtained from Promega. KI Jurkat cells were pelleted and washed with PBS and resuspended in CETSA media (Opti-MEM media supplemented with 1× Halt protease inhibitor cocktail) at 0.5×10^6/ml. 15µl of cell suspension was dispensed and pipet/mixed into each well of 384-well PCR plate using a robotic 384-channel pipette (Integra). 8-point dose gradient was created using hpD300e digital dispenser, and the final DMSO concentration was 0.2% v/v. Cell/compound mixture was incubated at 37℃ for 1 hour, then heat pulsed using a temperature gradient PCR thermocycler (Bio-Rad C1000 touch) using the following program: 5 min 20℃, 5 min temperature gradient and 5 min 20℃. For both DGKα and DGKζ, the temperature gradient was 39–63℃. 10 µl of Nano-Glo HiBiT lytic detection mix was pipet/mixed into the cell suspension after heat pulse and then analyzed with a bioluminescence plate reader (Perkin Elmer Envision with Ultra-Sensitive luminescence channel). Temperature response curve was analyzed with GraphPad prism Sigmoidal curve fitting. Melting temperature for each dose point was captured and analyzed using a dose response curve fitting.

Whole blood DGK potentiation assay

Human Whole blood was collected freshly (BMS internal donor program). 10 μL immune complex of 10 μg/mL anti-CD3 (BMS) and 40 μg/mL IgG cross-linker (ThermoFisher, Catalog# 31168) was added to 90 μL whole blood. After 15 minutes of incubation, the whole blood was fixed with Lyse/Fix buffer (BD Biosciences, Catalog# 558049). Cells were processed using Permeabilization III buffer kit (BD Biosciences, Catalog# 558050) and stained with antibodies specified in Supplementary Table S2. For IL-2 quantification, 10 μL immune complex of 10 μg/mL anti-CD3 and 40 μg/mL IgG cross-linker was added to 90 μL whole blood. After 24 hours of incubation, 10 μL whole blood was collected and diluted 1:1 with RPMI. IL-2 concentration was quantified by AlphaLISA Human IL-2 High Performance Detection Kit (Revvity, Catalog# AL3155C).

Western blotting of DGK degradation

To identify the mode of DGKα and DGKζ degradation, Jurkat cells were co-treated for 6h with the BMS-986408 with or without 1 μM bortezomib or 1 μM TAK-243 (MedChemExpress). Complete cell lysates were prepared using urea lysis buffer. The cell lysis buffer was made with 50 mM Tris-HCl (pH 8.0), 150 mM NaCl, 1 % NP-40, 2M urea and 1 × Halt protease inhibitor cocktail (ThermoFisher). 1–2 μg of total lysate were resolved and analyzed by the automated Simple western system (Peggy Sue, Bio-techne ProteinSimple). The primary antibodies for the Simple western included: recombinant Rabbit anti-hDGKA (Abcam, Catalog# ab243647), recombinant Rabbit anti-hDGKZ (Abcam, Catalog# ab239081) and Rabbit anti-human β-Actin (Cell Signaling Technologies, Catalog# 8457)

Syngeneic mouse tumor models efficacy study

At the time of tumor cell implantation (day 0), cells were harvested and ensured with ≥ 90% viability before implantation. For the MC38 model, female C57BL/6 mice at 8-10 weeks age were injected subcutaneously in the right flank with 1.0×10^6 of MC38 tumor cells resuspended in 0.1 mL PBS (ThermoFisher). For the CT26 model, female Balb/c mice at 8-10 weeks age were injected subcutaneously in the right flank with 1.0×10^6 of CT26 tumor cells in 0.1 mL PBS. For the SA1N model, female Balb/c mice at 8-10 weeks age were injected subcutaneously in the right flank with 1.0×10^6 of CT26 tumor cells in 0.1 mL PBS. Injection was performed using a 1 mL syringe and 26-gauge needle. At mean tumor volume of ~100 mm^3, animals were randomized into various treatment groups and treatment was initiated.

All compounds were formulated in a vehicle consisting of ethanol/polyethylene glycol 400 (PEG400)/tocopheryl polyethylene glycol succinate (TPGS) (5:90:5, v/v/v) for oral (PO) administration at 10 mL/kg dose volume. BMS-986408, DGKα-i and DGKζ-i were administered QD at final doses of 0.3 mg/kg, 5 mg/kg and 1 mg/kg, respectively. Anti-mPD-1 (BMS) were dosed intraperitoneally (IP) Q4D×3 at 10 mg/kg in a 10 mL/kg volume of phosphate-buffered saline (PBS). The isotype control for anti-PD-1 was mouse IgG1 (Bio X Cell, Catalog #BE0083) and was dosed IP at 10 mg/kg in a volume of 10 mL/kg PBS. Treatment groups were terminated when the mean tumor volume reached a target size of ≥1,000 mm^3 for two consecutive measurements. Tumor length (L) and width (W) were measured with calipers and tumor volumes were calculated using the formulation $L\times(W^2)/2$. If the mean tumor volume did not reach the target size, the treatment group was monitored for 10-times tumor volume doubling time.

MC38 Model Sample Processing and RNAseq Analysis

Bulk RNA sequencing was conducted at Azenta Life Sciences (South Plainfield, NJ, USA). Briefly, RNA was extracted from excised MC38 tumors from the tumor bearing mice post treatment using the RNeasy Plus Mini Kit (Qiagen, Hilden, Germany). Strand-specific RNA sequencing library was performed using the NEBNext Ultra II Directional RNA Library Prep Kit for Illumina following manufacturer's instructions (NEB, Ipswich, MA, USA). Sequencing was performed on an Illumina NovaSeq instrument according to manufacturer's instructions; using 2×150bp Paired-End (PE) reads configuration and targeting 50M reads per sample.

Paired-end reads were analyzed using the Seven Bridges platform (Seven Bridges Genomics). FASTQ reads were aligned to reference genome GRCm38 using STAR (16) with default parameters and transcriptome gene-level abundance estimated through RSEM (17) v1.1.13 with Ensembl GRCm38 v91 gene annotation. Downstream differential gene expression analysis was performed in R using the limma and voom R packages (18,19). Heatmap values were taken as the Z-score of log2 CPM values calculated through edgeR (20) with library normalization. Genes from the Nanostring Adaptive Immune Response Pathway of the nCounter PanCancer IO 360 gene panel (NanoString) were selected for heatmap visualization.

Tumor immuno-profiling by flow cytometry

MC38 tumors were collected seven days after the start of treatment and prepared as single cell suspensions using the Mouse Tumor Dissociation Kit (Miltenyi, Catalog# 130-096-730), according to the manufacturer's recommendations. Briefly, tumors were weighed and minced, then combined with the enzyme mixture in RPMI for enzymatic digestion and loaded onto a gentleMACS Dissociator for mechanical dissociation. Following dissociation, the samples were

filtered through 70-micron and 40-micron cell strainers to remove any remaining large particles and cell clumps and washed with media. Tumor-draining lymph nodes were collected at the same timepoint into RPMI media and were crushed with the plunger of a 3 mL syringe into a 40-micron cell strainer then rinsed with media.

For flow cytometry, cells were washed with PBS buffer and stained with viability dye (ThermoFisher, Catalog# L34976). After staining for cell surface markers, cells were washed with FACS buffer (PBS + 2% FBS + 2 mM EDTA). For intracellular staining, fixation/permeabilization buffer (ThermoFisher, Catalog# 00-5123-43) was used according to the manufacturer's directions to fix and permeabilize the cells, followed by intracellular staining. Single color compensation control beads were prepared using UltraComp Beads (ThermoFisher, Catalog# 01-2222-42) and used to calculate compensation, ensuring that any spread and spillover of fluorochromes into channels of interest were properly identified and corrected. Fluorescence minus one (FMO) samples were used to guide gating of different cell populations. The data for all samples was acquired using a cell analyzer (BD LSRFortessa™, BD Biosciences), and was analyzed with FlowJo version 10.4 (BD Biosciences) and graphed with GraphPad Prism (GraphPad Software). All antibodies used for flow cytometry are listed in Supplementary Table S2.

Nur77-GFP in vivo priming study

Nur77-GFP mice at 8-10 weeks age were injected subcutaneously in the right flank with 1.0×10^6 of MC38 tumor cells resuspended in 0.1 mL PBS. After tumor size reached $100mm^3$, mice were dosed with 1 mg/kg BMS-986408 orally with or without 10 mg/kg anti-PD-1 intraperitonially. On day after dosing, mice were sacrificed and the tumor draining lymph nodes were collected and processed with a 40-micron cell strainer then rinsed with RPMI. Flow cytometry was

performed to quantify the proportion of GFP^+ cells using a BD FACS Fortessa. Data was quantified with FlowJo (BD Biosciences).

OVA cross-presentation assay

Bone marrow cells from C57BL/6 mice (IQ Biosciences, Catalog# IQB-MBM201) were thawed and differentiated in RPMI media with 10% HI-FBS, 1% Pen/Strep, 1% Sodium Pyruvate and 1% NEAA and β-Me, supplemented with 40ng/ml mouse GM-CSF (Peprotech Catalog# 315-03). On day 3 and day 5 of incubation, half of the media was replaced and replenished with complete RPMI with 20ng/ml mouse GM-CSF. On day 7, immature mouse bone marrow–derived dendritic cells (BMDC) were collected by pipetting out the suspended and loosely adherent cells. Chicken Egg White Albumin (OVA; Sigma-Aldrich Catalog# A5503) was added to the cells to a final concentration of 5μg/ml. Meanwhile, spleens and total lymph nodes were collected from 3 OT-1 mice, pooled and processed with EasySep Mouse Pan Naïve T Cell Isolation Kit (Stemcell, Catalog# 19848A). The isolated total naïve OT-1 T cells were stained with CTV (ThermoFisher, Catalog# C34557) and then mixed with BMDC ± OVA in a 96-well plate. OT-1 to BMDC ratio was kept at 1:1. After 4 days of co-culture, the plate was spun down at 300g for 5min. The supernatant was collected for IL-2 quantification using a mouse IL-2 AlphaLISA Detection Kit (Revvity, Catalog# AL585C). The cell pellet was analyzed by flow cytometry with the antibodies listed in Supplementary Table S2.

NY-ESO-1 T cell Tumor Killing Assay

NY-ESO-1 T cells were generated by lentiviral transduction of human primary T cells. T cells were purchased from BioIVT as frozen stocks. Frozen T cells were thawed and cultured in RPMI with 10% HI-FBS, sodium pyruvate, NEAA HEPES (ThermoFisher), 10ng/ml human IL-2

(Peprotech, Catalog# 200-02), 5 ng/ml human IL-7 (Peprotech Cat# 200-07) and 5ng/ml human IL-15 (Peprotech, Catalog# 200-15). Cells were stimulated with Dynabeads Human T-Activator (ThermoFisher, Catalog# 111.32D) with beads:T ratio of 3:1. After overnight of stimulation, the T cells were transferred to a 6-well plate at 2.4×10^6 cells/well, and infected with lentivirus expressing human NY-ESO-1 TCR at MOI of 10. The lentivirus was purchased from Flash Biosolutions. The cells were centrifuged for 2 hours, 37°C at 800g, and then transferred back to an incubator. After 3 days, the cells were collected and the Dynabeads were removed by magnets. Transduced cells were expanded in larger culture volumes supplemented with fresh human IL-2, IL-7 and IL-15 every day. On day 11, the expanded NY-ESO-1 T cells were harvested for next step uses.

SAOS2-GFP/Luc cells were seeded in a 384-well ViewPlate (Perkin Elmer) using a multidrop combi dispenser and incubated for a few hours until adhesion (37°C, 10% CO_2). Compounds were dispensed by Tecan D300e followed by addition of 20ul of NY-ESO T cells at the pre-determined effector to target ratio of 1:2. Co-cultures were then incubated for 72h (37°C, 5% CO_2), followed by spin, removal of culture medium using a Biotek washer, resuspension of cell pellet and addition of ONE-Glo EX Luciferase reagent (Promega) per the manufacturer's instructions. Luminescence was measured using an Envision (Perkin Elmer) plate reader.

In vitro TRP1 $CD8^+$ T-cell priming assay

Antigen-presenting cells were isolated from C57BL/6 splenocytes. Briefly, spleen was collected from C57BL/6 mice and mechanically homogenized through 40-μm filters, and B cells were isolated via negative selection with mouse CD43 magnetic Dynabeads (ThermoFisher, Catalog# 11422D) and activated with anti-mouse CD40 agonist (clone HM40-3) for 2 days. On day 2, B cells were pulsed with the native Trp1 peptide (50pg/mL) TAPDNLGYA, as previously

described (21). Concurrently, cells were harvested from the spleen and inguinal lymph nodes of the TRP1^{high}Rag2$^{-/-}$ mice (22), and CD8^{+} T cells were isolated using the EasySep Mouse CD8^{+} T cell isolation kit (Stemcell Technologies, Catalog# 19853) following as per the manufacturer's protocol. CD8^{+} T cells were stained with CTV (ThermoFisher, Catalog# C34557). T cells and antigen-presenting cells were cocultured in a 96-well U-bottom plate at a 2:1 T:B cell ratio in RPMI complete media supplemented with human IL-2 (100 U/ml) (PeproTech). Proliferation was quantified via a proliferation index representing the fraction of mitotic events by the number of progenitor cells. Proliferation index was calculated as previously described (4).

TRP1^{high} and TRP1^{low} priming in mice bearing C2VTrp1 tumors

Spleen and lymph nodes were collected from TRP1^{high} Rag2$^{-/-}$ mice and TRP1^{low} Rag2$^{-/-}$ mice, and CD8^{+} T cells were isolated using EasySep Mouse CD8^{+} T cell isolation kit (Stemcell Technologies, Catalog# 19853) following as per the manufacturer's protocol. CD8^{+} T cells were stained with CTV (ThermoFisher, Catalog# C34557). The CTV stained CD8^{+} T cells were resuspended in endotoxin-free PBS (ThermoFisher). C57BL/6 mice were irradiated with 100 rad and 6 hours later received tail vein injections of approximately 2×10^{6} TRP1^{high} and 1×10^{6} TRP1^{low} T cells. The following day, mice were inoculated with 250,000 C2VTrp1 tumor cells in endotoxin-free PBS. Five days after tumor inoculation, mice were euthanized, and the draining inguinal lymph node was collected. Lymph nodes were digested as follows. Each lymph node was placed and pierced with forceps in RPMI 1640 media supplemented with Dispase II (0.8 mg/ml; Life Technologies, Catalog# 17105041), collagenase P (0.2 mg/ml; Sigma-Aldrich, Catalog# 11249002001), and deoxyribonuclease I (DNase I) (0.1 mg/ml; Sigma-Aldrich, 10104159001). Lymph nodes were incubated in this media for 30 min at 37°C. After complete digestion, the solution containing Dispase II, collagenase P, and DNase I was neutralized with

FACS buffer containing 2% FBS and 2 mM EDTA in PBS. Cells were then stained with antibodies listed in Supplementary Table S2, and samples were recorded using Sony SP6800 spectral flow cytometer.

Human PBMC assay and synergy analysis

Human PBMCs were purchased from Stemcell (Catalog# 70025). Cells were resuspended in complete RPMI (RPMI + 10% FBS + NEAA + Sodium Pyruvate + β-Mercaptoethanol) to a concentration of 50,000 cells/mL. For sub-optimal T-cell activation, anti-CD3 (clone OKT3; Biolegend, Catalog# 317326) was added to the PBMC suspension to a final concentration of 0.01ng/ml. The cells were aliquoted to 384-well cell culture plates at 50ul/well (2500 cells/well) using Combi Multidrop (ThermoFisher). DGK inhibitor compounds were matrix-dispensed to the plate with Tecan D300e dispenser. Cell proliferation and cytokine analysis was performed on day 6 of culture. T-cell proliferation in PBMC was quantified with CTG 2.0 (Promega, Catalog# G9241). For cytokine profiling, 10ul/well supernatant was collected from each well and IFN-γ release was quantified by human IFN-γ AlphaLISA Detection Kit (Revvity, Catalog# AL217F). Briefly, acceptor beads and biotinylated antibody were diluted with working buffer, and 8µl/well samples were loaded onto a white OptiPlate-384 plate (PerkinElmer). 4µl/well of testing supernatant or standard were added. After 1 h incubation, 8µl/well diluted donor beads were loaded onto the assay plate. After another 30 min incubation, plates were read using an Envision with Mirror D640as (444), plus Emission Filter M570w (244) or Emission Filter M615 (203).

For synergy calculation between DGKα-i and DGKζ-i, the mean values of either the proliferation signal or the IFN-γ signal were derived from 6 biological replicates. The data was then reformatted in the SynergyFinder accepted format, and processed with SynergyFinder (23) online portal (https://synergyfinder.org/). The Highest Single Agent (HSA) plots were exported.

Primary T-cell Phosphoproteomics

Human $CD4^+$ T cells were isolated from human PBMCs and stimulated in a T75 flask pre-coated with 1.5μg/ml anti-human CD3 (clone G19.4.2.5; BMS internal). Cells were cultured in complete RPMI, supplied with 1μg/ml anti-human CD28 (clone 9.3; BMS internal). After 3 days of initial culture, media was refreshed and supplemented with 10 Unit/mL human IL-2 (Peprotech, Catalog# 200-02). Cells were further expanded to day 13 with the media refreshed on day 6 and day 10. After 13 days of expansion, rested CD4+ T cells were collected and frozen down for storage. On day of study, expanded CD4+ T cells were thawed and seeded in 96-well plates and treated with Dynabeads™ CD3 (ThermoFisher) at beads:T ratio of 1:1 for 15 min followed by the indicated compounds for 60 min. Tryptic lysates were prepared for proteomic data acquisition using the ist-BCT 96 sample kit (PreOmics, Catalog# PO00067). Phosphopeptide samples were then enriched using Agilent Bravo with Fe(III) NTA cartridges tips (Agilent, Catalog# G5496-60085) followed by data collection using an LC-MS/MS system (Evosep, Catalog# EV-1000) that was connected online to a mass spectrometer (Bruker, timsTOF SCP). For the LC-MS/MS workflow, peptides were loaded on to an 15cm reverse phase column (EV-1137) (15cm x 150μm ID, 1.5μm C18) joined to a 20μm ZDV captive spray emitter (PR10781883-V2). An EVOSEP One (EV-1000) System (EVOSEP) was directly coupled online with the mass spectrometer (Bruker timsTOF SCP) via electrospray source set to 1600V. Peptides were separated with a binary buffer system of Buffer A (0.1% Formic Acid in Water) and Buffer B (0.1% Formic Acid in Acetonitrile) using the EVOSEP 30SPD method (44 min gradient at 500 nL/min). Data is collected in positive ion mode with a Data Independent Parallel Accumulation Serial Elution Fragmentation mode setting (DIA-PASEF).

Peptide identification and relative quantification were performed using DIA-NN 1.8.1(24) with an in silico library generated from UniProt database. Precursor data obtained from DIA-NN was re-summarized using the tidyverse package. Briefly, each peptide was grouped by its root sequence, charge state, number of phosphorylations, and protein group to create unique precursor group identifiers, and the quantitative data were summarized by calculating the mean across observations within each group. The re-summarized data was then subjected for dose-response analysis by fitting nonlinear regression models using the LL.4 method from the drc package (25). The significance of dose dependency across the peptide data was assessed by a chi-square test. The resulting p-values served as an effect size metric, which was further used for ranking and nomination of phosphorylation sites based on their response to varying treatment doses. Pathway enrichment was conducted using Kinase inference analysis with KinSwingR (Waardenberg A (2024). KinSwingR allows network-based kinase activity prediction. R package version 1.22.0.). In the kinase inference analysis, the phospho-peptides were mapped from the Phosphosite kinase substrate motif library (https://www.phosphosite.org/homeAction.action).

NSCLC scRNAseq analysis

We collected the integrated scRNAseq data published by Lim et al. (26), containing 224,611 cells from human primary NSCLC tumors. In that study, the authors had pre-processed and integrated seven independent scRNAseq datasets using an anchor-based approach, with five datasets utilized as reference and the remaining two as validation. For our study, the cell types were filtered based on the original authors' annotation labels and we only included immune cells in our analysis. The expressions of selected genes were plotted with Seurat R library.

Multiplexed immunofluorescence of NSCLC patient tumors

NSCLC patient cancer tissue microarrays were acquired from BioChain Inc. Four microarrays, comprising a total of 112 tissue cores from 56 patients were used for the multiplexed immunofluorescence study. All the microarray samples were sliced from FFPE-processed tissues to 4 μm sections. The slides were baked for 1 hour at 62 degrees Celsius (VWR Oven Gr Con 2.3CF, 89511-404) in a vertical slide orientation rack with subsequent deparaffinization (Leica, Bond Dewax Solution, AR9222). Antigen retrieval was performed for 32 minutes using Bond ER2 (Leica, AR9640) at 100°C on the Leica Bond RX automated research strainer. A Lunaphore COMET imaging chip (MK03) was placed over the intended acquisition region according to user alignment with regions pre-selected on an adjacent H & E stained slide. A slide with a mounted COMET chip was loaded into the COMET device (PA Model) followed by acquisition of the first cycle of autofluorescence imaging followed by 20 cycles of staining, imaging, and elution. Each cycle contained one rabbit and/or one mouse primary antibody detected with an Alexa Fluor conjugated species-specific secondary antibody (Supplementary Table S2). All secondary antibodies were incubated for 4 minutes. The optimal antibody concentration, marker cycle position in the panel and incubation time for each primary antibody (8 minutes for CD25, CD45RO, TIGIT, CD1C and FOXP3 and 4 minutes for all other primary antibodies) was optimized such that the results of the multiplex imaging were semi-quantitatively concordant with the sensitivity and specificity of a correlative, optimized single diaminobenzidine (DAB) immunohistochemistry (IHC) stain across multiple control tissues. Standard IHC was performed on the Leica BondRx using the Leica BOND Polymer Refine Detection Kit, DS9800. For COMET, all antibodies were pre-diluted with Intercept Antibody Diluent (LI-COR, Catalog# 927-65001). After each staining cycle, elution of primary and secondary antibodies was

performed with Elution Buffer Solution (Lunaphore, Catalog# BU07-L) for 4 minutes. Regions of interest measuring 9mm^2 were selected at a 200× final magnification and imaged under the Lunaphore slide cover chip for each sample and a full channel stacked OME.tiff file was generated automatically upon completion. The OME.tiff image was exported after autofluorescence background subtraction using Horizon Viewer (version 2.2.0.1) Lunaphore COMET Viewer software and was visualized and assessed per channel using Indica Lab HALO softwareHALO platform by Indica Lab (HALO version 3.6.4134.396 and HALO AI version 3.6.4134) to ensure single cell alignment fidelity, followed by cell segmentation. Signal marker thresholding was subsequently performed separately on each TMA core. Binary classification (positive or negative) was determined for each cell object in HALO.

Cell phenotypes were defined as explicit combinations of positive and negative markers (Supplemental Table S2). Fluorescence intensity (cytoplasmic intensity for cytoplasmic markers or nuclear intensity for nuclear markers) was normalized as follows: within a given core, for a given marker, intensity values were divided by the minimal intensity value corresponding to a "positive" binary classification. Subsequently, all values less than 1 were set to 1. Normalized intensity values were then log2 transformed for downstream analysis. Marker correlation p-values were adjusted for multiple hypothesis testing using the Benjamini-Hochberg method. Fluorescence intensity normalization and subsequent analyses were performed using R Statistical Software (v4.3.2; R Core Team 2023).

NSCLC PDOTs generation, cytokine analysis and flow cytometry

NSCLC PDOTs were obtained from 10 patients treated at Massachusetts General Hospital (MGH) and DFCI. Written informed consent was obtained from all subjects. Tumor samples were collected and analyzed according to Dana-Farber/Harvard Cancer Center Institutional

Review Board approved protocols (IRB 98-063 and IRB 02-180). PDOTS were generated as previously described (27,28). Briefly, fresh NSCLC tumor specimens were chopped in a 15 mL falcon tube in prewarmed to 37C full media (DMEM + 10% FBS + 50 U/mL Penicillin-Streptomycin + 100 U/mL collagenase type IV (ThermoFisher, Catalog# 17104019) and 50 μg/mL DNase I (Roche #10104159001) for approximately 15 minutes using sterile scissors and trituration. Dissociated material was sequentially strained through 100-μm filter and 40-μm filters to generate PDOTs fractions containing single cells (S3) and organotypic spheroids that are either > 100 μm (S1) or 40-100 μm (S2). S1 material was cultured in ultralow-attachment (ULA) tissue culture plates (Corning). After 3 days in culture with 100 μg/mL Nivolumab with or without 250 nM BMS-986408, S1 fractions were further dissociated using a gentleMACS^{TM} Octo Dissociator with Heaters and Tumor Dissociation Kit, human (Miltenyi), which was performed according to the manufacturer's instructions. Cytokine analysis of conditioned media from S1 cultures after 3 days of treatment was performed using the MSD U-PLEX Viral Combo 1 assay (Hu: K15343K-2) according to the manufacturer's instructions. For flow cytometry, red blood cells were removed from the samples using red blood cell lysis buffer (BioLegend, Catalog# 420301). Samples were pelleted and then resuspended in PBS and strained through a 40μm filter. Cells were incubated with the Live/Dead Zombie NIR (Biolegend, Catalog# 423105) for 5 minutes in the dark at room temperature. Fc receptors were blocked prior to surface antibody staining using Human TruStain FcX Blocking Reagent (BioLegend, Catalog# 422301). Cells were stained with antibodies (Supplementary Table S2) for 15 minutes on ice in the dark and washed 2× with PBS + 2% FBS. Cells were analyzed on a BD LSRFortessa with FACSDiva software v9.0 (BD Biosciences). Data were analyzed using FlowJo software version 10.8.1.

CAR T-cell generation

$CD4^+$ and $CD8^+$ T cells were isolated from human apheresis donors using immunomagnetic selection (ClinicMACS Plus, Miltenyi Biotec) and frozen. $CD4^+$ and $CD8^+$ T cells from individual donors were later thawed, and combined at a 1:1 ratio. CAR T-cells were manufactured with a proprietary activation step and subsequent lentiviral transduction with an anti-CD19 CAR which includes CD3ζ signaling and 4-1BB costimulatory endodomains. CAR T-cells with knockouts were engineered using CRISPR-Cas9 to contain a knockout for DGKα, DGKζ or both DGKα and DGKζ. Knockouts were verified by sequencing the target locus. All CAR T products from each donor were expanded in cytokine-enriched media, cryopreserved, and stored in the liquid nitrogen vapor phase until ready for use. The human CAR T-cell production described in this publication did not involve a clinical investigation in human participants nor did it involve the use or collection of any identifiable personal information; therefore, institutional review board (IRB) review and approval was not required for the performance of the research. Human materials used in this research were received by the researchers in a fully deidentified manner from commercial repositories.

CAR T-cell Chronic Stimulation and Proliferation Assay

CAR T-cell products were thawed, rested at 37°C for 45-60 minutes and then counted on a Nexcelom Biosciences Cellometer Auto 2000 Counter using acridine orange and propidium iodide (AO/PI) nuclear staining solution (ViaStain, CS2-0106-5mL). Cells were seeded based on $\%CAR^+$, as determined by flow cytometry, into either a medium throughput (24W G-Rex® with in-house anti-idiotypic M450 CAR stimulus beads) or high throughput (96W non-TC flat-bottom plate coated with in-house anti-idiotypic CAR stimulus) chronic stimulation assay. Fold change

of expansion in the medium throughput assay was calculated based on 48hr live cell counts divided by the total number of cells seeded at the beginning of the assay.

CAR T-cell 3D Spheroid Cytotoxicity Assay

Cytotoxicity was measured using the Incucyte S3 Live-Cell Analysis System (Sartorius) and target expressing cell lines that had been engineered to fluoresce, A549-CD19/NucLightRed® or Granta-519/NucLightRed®. Target cells were seeded at $5x10^3$ per well into SBio PrimeSurface 3D cell culture round-bottom plates (SBio, Catalog# MS-9096UZ) and allowed to form a spheroid. CAR^+ cells were then added to each well according to %CAR+. Both phase and red fluorescence images were acquired by 4× objective every 12 hours for the duration of the assay. For rescue assays, chronically stimulated CAR T cells were removed from stimulus and seeded directly into 3D cytotoxicity assays with varying treatment levels of BMS-986408. Tumor spheroid area was assessed at day 9 to determine significant differences.

CAR T-cell flow cytometry

For in vitro flow cytometry analysis, live cells were aliquoted into a 96-well plate, pelleted at 1000g for 1 minute and stained with Near-IR live/dead distinguishing cell dye (ThermoFisher, Catalog# L10119). Cells were then washed and stained according to standard surface staining procedure in Cell Staining Buffer (Biolegend, Catalog# 420201). For intracellular staining, T-cell culture media contained 1× Protein Transport Inhibitor Cocktail (ThermoFisher, Catalog# 00-4980-93) and cells were treated for 5 hours prior to beginning staining. Following live/dead and surface staining, cells were fixed, permeabilized and stained with intracellular antibodies. Polyfunctionality was determined by gating triple-cytokine producing CAR T cells (IFN-γ^+, IL-2^+, TNF-α^+). To measure expression of costimulatory markers on Granta-519, K562-CD19,

Nalm-6, and Raji cell lines, cells from growing cultures were aliquoted into a 96-well plate, pelleted at 1,000g for 1 minute and stained with Near-IR live/dead distinguishing cell dye. Cells were then washed and stained according to standard surface staining procedure in Cell Staining Buffer® with anti-CD40, anti-41BB, anti-CD80 and anti-CD86 antibodies conjugated to fluorochromes and analyzed on a BD FACSymphony A5 SE Cell Analyzer (BD Biosciences) and analyzed with FlowJo version 10.6 (BD Biosciences).

For flow cytometry analysis of samples from mice treated with CAR T-cells, 0.2mL blood was collected via retro-orbital sinus from anesthetized mice on days 5, 12, 19 and 26 (Raji) or days 8, 16, 23, and 30 (Nalm6). Blood was transferred into EDTA-coated blood collection tubes (BD Biosciences, Catalog# 365974) and briefly centrifuged. Blood was transferred to a 96-well plate, mixed with 1mL of red blood cell lysis buffer (Biolegend, Catalog# 420301) and incubated at room temperature for 20 minutes. Samples were centrifuged at 1500rpm for 5 minutes. The supernatant was removed and cells were resuspended in Cell Staining Buffer (Biolegend, Catalog# 420201) and transferred to a new 96-well plate. Cells were stained with Near-IR live/dead distinguishing cell dye and subsequently stained for cell surface markers using the antibodies in Supplementary Table S2. Single color compensation control beads were prepared using UltraComp Beads (ThermoFisher, Catalog# 01222242) and used to calculate compensation. The data for all samples was acquired using a BD FACSymphony A5 SE Cell Analyzer (BD Biosciences) and analyzed with FlowJo version 10.6 (BD Biosciences).

Raji and Nalm6 *in vivo* study

Raji and Nalm6 cells were grown and maintained according to ATCC guidelines. Prior to injection, cells were grown to 70% confluence at which point they were harvested and prepared for intravenous injection. For in Life Tumor Monitoring, female NSG mice aged 8 weeks were

injected intravenously with 5.0×10^5 luciferase expressing Raji cells or 4.0×10^5 luciferase expressing Nalm6 cells (day 7 for Raji, day 4 for Nalm6) and animals were randomized into various treatment groups. Imaging of mice was performed with the Xenogen IVIS® imaging system (Perkin Elmer, Waltham, MA) and IP administration of D-Luciferin at 15mg/kg (Perkin Elmer, Catalog# 122799). Bioluminescence imaging was used to quantify tumor burden for both Raji and Nalm6 studies. For CAR T-cell therapy, frozen CAR T-cells, previously engineered as described above, were thawed, washed, counted, and resuspended in PBS. In both Raji and Nalm6 studies, CAR T-cell groups received a suboptimal dose of 1.0×10^6 CAR^+ cells per mouse via intravenous injection. For treatment, BMS-986408 was formulated in a vehicle consisting of ethanol/polyethylene glycol 400 (PEG400)/tocopheryl polyethylene glycol succinate (TPGS) (5:90:5, v/v/v) for PO administration at 0.3mg/kg. BMS-986408 was administered QD×28 at a dose of 0.3mg/kg starting on day 0. For Modified Tumor Control Index calculation, the index was derived from the tumor control index (29), which compiles three scores per experimental group assessing tumor inhibition, stability, and rejection. We modified this method to calculate the three sub scores for each individual mouse, an improvement that allows for statistical analysis between experimental groups.

CAR T-cell study cytokine quantification

Cytokine production was quantified by MSD UPLEX assays (Mesoscale Discovery) according to the manufacturer's protocol. Quantification of cytokines in supernatant collected from A549-CD19 or Granta-519 CAR T-cell co-cultures was performed using the Meso Scale Discovery (MSD) 10-plex assay using the Proinflammatory Panel 1 Multiplex Test Kit. All samples were evaluated in duplicate at standard 1:2 dilution and maximal 1:8 dilution; calculated percentage coefficients of variation for the duplicate measures were less than 20%.

Data and Code Availability

RNAseq data for the MC38 model has been deposited to Gene Expression Omnibus (GSE293295). R code for scRNAseq analysis is provided in the GitHub repository (https://github.com/flycat1989/DGK_scRNAseq). All other data are available in the manuscript and its accompanying supplementary files or from the corresponding author upon reasonable request.

Results

BMS-986408 is a potent dual DGKα/ζ inhibitor that broadly amplifies T-cell activation

DGKs are a large family of lipid kinases containing 10 isozymes divided into five types (30). In T cells, DGKα (type I family) and DGKζ (type IV family) are the most prevalent isozymes (8,9). BMS-986408 (Fig. 1A) showed potent inhibition of both recombinant DGKα (IC_{50} 0.0003 μM) and DGKζ (IC_{50} 0.002 μM) lipid kinase activity (Fig. 1B) and inhibited the cellular conversion of labelled DAG to PA in Jurkat T cells (Fig. 1C). Among the type I family, BMS-986408 showed > 100-fold selectivity for DGKα over DGKβ and DGKγ (Supplementary Fig. S1A). Among the type IV family, BMS-986408 inhibited DGKζ and DGKι with similar potency (Supplementary Fig. S1A). No significant activity was observed for Type II (DGKδ, DGKη, DGKκ), Type III (DGKε) or Type V (DGKθ) family members (Supplementary Fig. S1A). Direct binding to DGKα and DGKζ in cells was confirmed using a NanoBRET assay where a BMS-986408–derived tracer showed rapid and specific binding to both DGKα and DGKζ (Fig. 1D and E). Target engagement was further confirmed with a CETSA where BMS-986408 reduced the thermal stability of both DGKα and DGKζ (Fig. 1F). Previously, we showed DGK inhibitors from this chemical series induced plasma membrane translocation (3). This mechanism of action was shown to be independent of known mediators of DGKα translocation including SRC phosphorylation of DGKα Y335 and calcium flux (3). As expected, BMS-986408 also induced the translocation of both YFP-DGKα (EC_{50} 0.026 μM) and YFP-DGKζ (EC_{50} 0.008 μM) from cytoplasm to plasma membrane (Fig. 1G and H). Through the evaluation of DGKα and DGKζ protein levels, we discovered that BMS-986408 also induced the degradation of both DGKα and DGKζ (Fig. 1I). Degradation was reversed with ubiquitination (E1i; TAK-243) and

proteosome (BZ; Bortezomib) inhibitors, confirming that BMS-986408–mediated degradation of DGKα and DGKζ was both ubiquitin and proteosome dependent (Fig. 1J).

BMS-986408 potency in primary T cells was assessed in human whole blood with sub-optimal CD3 activation and phospho-ERK and IL-2 were measured as pharmacodynamic biomarkers of DGKα/ζ inhibition (Fig. 1K). BMS-986408 showed potent amplification of phospho-ERK in both $CD4^+$ (EC_{50} 0.008 μM) and $CD8^+$ (EC_{50} 0.012 μM) T cells (Fig. 1L) and IL-2 production (Donor 1 EC_{50} 0.019 μM; Donor 2 EC_{50} 0.034 μM) (Fig. 1M). BMS-986408 amplified the antigen-specific activation of naïve mouse OT-1 $CD8^+$ T cells by autologous BMDCs cross-presenting OVA, as measured by proliferation (EC_{50} 0.015 μM) (Fig. S1B and S1C) and IL-2 production (EC_{50} 0.022 μM) (Fig. S1D). BMS-986408 also amplified the antigen-specific killing of NY-ESO-1 antigen presenting SAOS-2 cells by human T cells transduced with NY-ESO-1 TCR (EC_{50} 0.001 μM) (Fig. S1E and S1F). These results showed that BMS-986408 can broadly amplify T-cell responses with translatable potency across human and mouse cellular assays.

BMS-986408 binds to the accessory subdomain of the DGKα and DGKζ catalytic domain

We next focused our efforts on elucidating the BMS-986408 binding site; however, there were currently no solved structures for full-length protein or the kinase domains of mammalian DGKα or DGKζ by NMR, X-ray crystallography, or cryo-EM (31) and our attempts to obtain structures of BMS-986408 with DGKα or DGKζ were unsuccessful. To overcome this hurdle, we designed a genomic approach using CRISPR-mediated base editing (32) paired with flow cytometry to enrich for mutants resistant to BMS-986408–mediated DGKα/ζ degradation (Fig. 2A). This approach identified a clustering of sgRNAs within the accessory subdomain of the catalytic domain of both DGKα (Fig. 2B) and DGKζ (Fig. 2C). The mutations were mapped onto

the AlphaFold predicted structures of DGKα (Fig. 2B) and DGKζ (Fig. 2C). Three mutations for DGKα (S532P, L556P and H606R) and DGKζ (F463S, S490P and C534R) (highlighted in green in Fig. 2B and C) were selected for further validation, based on both Log2 fold change (LFC) in sgRNA enrichment and location within the putative binding sites. Endogenous knock-in mutation reporter cell lines were generated, and all these mutations conferred resistance to BMS-986408–mediated degradation (Fig. 2D). Additionally, these mutants abrogated BMS-986408 cellular binding as measured by CETSA (Fig. 2E and F). Induced-fit docking models (33) were generated for both DGKα and DGKζ showing the binding pose by ribbon/stick representation (Fig. 2G) and electrostatic surface (Fig. 2H). Without three-dimensional structures, structural insight into mammalian DGKα and DGKζ has been achieved through comparison with distantly related prokaryotic DGKs such as *Staphylococcus aureus* DgkB and mammalian lipid kinase including Sphingosine kinase 1 (34). The proposed BMS-986408 binding site overlapped with the lipid binding sites of both proteins (Supplementary Fig. S2A) and biochemical studies confirmed that BMS-986408 is a DAG substrate competitive inhibitor (Supplementary Fig. S2B). A summary of the BMS-986408 mechanism of action is presented in Supplementary Fig. S2C.

DGKα/ζ inhibition unleashes PD-1 T Cell Immune Checkpoint Therapy

DGKα/ζ inhibition is of particular interest in the context of anti-PD-1 therapy as DAG metabolism operates downstream of PD-1 signaling (Fig. 3A) presenting a potentially major roadblock to therapeutic benefit. To evaluate the therapeutic potential of BMS-986408, we tested the efficacy of BMS-986408 in combination with anti-PD-1 therapy. We selected syngeneic tumor models responsive to anti-PD-1 therapy, but with varying depth and durability of tumor regression, and focused on complete tumor regression (CR) as the primary measure of response.

Anti-PD-1 monotherapy (10 mg/kg Q4D×3) showed a CR frequency of 40%, 10%, and 0% in SA1N (Fibrosarcoma), MC38 (Colorectal) and CT26 (Colorectal) tumor models, respectively (Fig. 3B). BMS-986408 (0.3 mg/kg QD×28) monotherapy exhibited tumor growth inhibition across all three models but was incapable of eliciting CRs (Fig. 3B). However, anti-PD-1 and BMS-986408 combination produced a robust therapeutic response with 90-100% CR across all three models (Fig. 3B).

Next, we evaluated how these therapies impacted T-cell responses in tumors and tumor-draining lymph nodes (TdLNs). Bulk RNAseq analysis of MC38 tumors showed that while both anti-PD-1 and BMS-986408 monotherapies induced transcriptomic changes, the combination led to a robust increase in both the number and magnitude of differentially expressed genes (Fig. 3C and D; Supplementary Table S3). This included the upregulation of $CD8^+$ T-cell effector genes *Ifng* (IFNγ), *Tnf* (TNFα), *Gzma* (Granzyme A), *Gzmb* (Granzyme B), *Prf1* (Perforin), *Lamp1* (CD107a) and *Fasl* (Fas Ligand) (Fig. 3D). Flow cytometric profiling showed that only the combination therapy significantly increased the frequency of Granzyme B^+ (effector) and $Ki67^+$ (proliferating) $CD8^+$ T cells in the MC38 tumors (Fig. 3E). In CT26 tumors, anti-PD-1 and BMS-986408 combination therapy increased the proportion of AH1 tumor antigen–specific $CD8^+$ T cells within the tumors, and the frequency of $CD69^+$ (activated) $AH1^+CD8^+$ T cells was also increased (Supplementary Fig. S3).

In MC38 TdLNs, BMS-986408 monotherapy induced multiple biomarkers of $CD8^+$ T-cell activation including: 1) reduced naïve $CD8^+$ T cells, 2) increased effector/effector memory and central memory $CD8^+$ T cells, and 3) increased frequency of both activated ($CD69^+$ and $PD\text{-}1^+$) and proliferating ($Ki67^+$) $CD8^+$ T cells (Fig. 3F). Anti-PD-1 monotherapy did not induce these same changes and provided no combinational benefit over BMS-986408 alone (Fig. 3F).

Next, we tracked $CD8^+$ T-cell priming in MC38 TdLNs implanted into Nur77-GFP transgenic mice where newly primed T cells express GFP (35). BMS-986408 increased the frequency of GFP^+CD8^+ T cells while anti-PD-1 had no significant impact (Fig. 3G).

To test the antigen-specific response with various TCR affinities, we labelled $CD8^+$ T cells with either a high ($TRP1^{high}$) or a low ($TRP1^{low}$) affinity TRP1-specific TCR, and adoptively transferred cells into C2VTrp1 tumor bearing mice. $TRP1^{high}$ and $TRP1^{low}$ $CD8^+$ T cells migrate into TdLNs where proliferation can be assessed by CTV dilution (4,22). BMS-986408 monotherapy markedly improved the proliferation of both $TRP1^{high}$ and $TRP1^{low}$ $CD8^+$ T cells (Fig. 3H and I) while anti-PD-1 provided no monotherapy or combination benefit (Fig. 3H and I). These results showed that BMS-986408 works in concert with anti-PD-1 T-cell immune checkpoint therapy to unleash T-cell responses in the tumor while also providing the benefit of amplifying the priming and expansion of tumor-reactive T cells in TdLNs.

Inhibiting both DGKα and DGKζ is necessary to maximize combination benefit with PD-1

We and others have reported through genetic studies that both DGKα and DGKζ isozymes regulate T-cell signaling, function and tumor immunity (11). However, the relative contribution of therapeutically targeting DGKα, DGKζ or both can only be parsed with pharmacologic inhibitors. Toward this goal, we synthesized DGKα (DGKα-i) and DGKζ (DGKζ-i) inhibitors (Supplementary Fig. S4A) and confirmed their activity in DGK lipid kinase assays (Supplementary Fig. S4B), DGK CETSA (Supplementary Fig. S4C and S4D), and DGK translocation assays (Supplementary Fig. S4E and S4F). Next, we evaluated these inhibitors in combination with PD-1 therapy in the MC38 tumor model. While anti-PD-1 monotherapy provided modest therapeutic benefit with a CR frequency of 15%, combination with BMS-986408 (dual DGKα/ζ inhibitor) improved the CR frequency to 92% (Fig. 4A). The DGKα-

i/anti-PD-1 combination did not improve therapeutic benefit compared with anti-PD-1 monotherapy while the DGKζ-i/anti-PD-1 combination provided a modest improvement (30% CR) (Fig. 4A). Moreover, co-administration of both DGKα-i and DGKζ-i with anti-PD-1 improved the therapeutic benefit to 100% CR, which was comparable to dual DGKα/ζ inhibition with BMS-986408 (Fig. 4A). These data showed that inhibiting both DGKα and DGKζ was necessary to maximize the combination benefit with PD-1 therapy.

We next turned to cellular assays to understand how DGKα and DGKζ inhibition might differentially contribute to $CD8^+$ T-cell effector and priming responses. All three inhibitors improved antigen-specific killing of NY-ESO-1 TCR transduced human T cells (Fig. 4B) and the rank order for improvement in cytotoxicity was dual DGKα/ζ > DGKζ-i > DGKα-i (Fig. 4B). These data showed that while DGKζ was more dominant than DGKα in regulating T-cell cytotoxicity, dual inhibition was required to maximize the response potential. In cellular priming/proliferation assays with either human (PBMCs) or mouse ($TRP1^{high}$ $CD8^+$) T cells, all three inhibitors improved the proliferation response (Fig. 4C) and the rank order for improvement in response was again dual DGKα/ζ > DGKζ-i > DGKα-i (Fig. 4C). Particularly in human PBMCs, the dual DGKα/ζ inhibitor BMS-986408 significantly outperformed either DGKζ-i or DGKα-i (Fig. 4C). We next evaluated T-cell proliferation *in vivo* by measuring the expansion of adoptively transferred $TRP1^{high}$ $CD8^+$ T cells in the TdLNs of mice bearing C2VTrp1 tumors. *In vivo*, only dual DGKα/ζ inhibition by BMS-986408 improved the proliferation of $TRP1^{high}$ $CD8^+$ T cells (Fig. 4D). These results showed that targeting both DGKα and DGKζ is necessary to improve T-cell priming.

To further elucidate the interplay between DGKα and DGKζ inhibition, we performed a matrixed dose titration of the DGKα-i and DGKζ-i in human PBMCs under sub-optimal T-cell

stimulation conditions. DGKα-i and DGKζ-i demonstrated considerable synergy with average higher than single agent (HSA) (36) scores of 15.07 for proliferation (Fig. 4E) and 15.08 for IFNγ production (Fig. 4F). We next used global phosphoproteomics to deconvolute the impact of DGKα, DGKζ and dual DGKα/ζ inhibitors on the TCR signalosome following T-cell activation. BMS-986408 resulted in much greater signal effect size than either DGKα-i or DGKζ-i (Fig. 4G and Supplementary Fig. S5A; Supplementary Table S4). Pathway analysis revealed dual inhibition induced the phosphorylation of proteins enriched in the TCR signaling cascade, namely the NF-κB and MAPK pathways (Fig. 4H and I), which are downstream of DAG signaling in T cells (3,37,38). Examples of the targets with increased phosphorylation included PRKCQ and NFKB2 in the NF-κB pathway and ARAF, BRAF, and MAP3K3 in the MAPK pathway (Fig 4I, Supplementary Fig. S5B and S5C). The enhanced phosphorylation of PRKCQ (PKCθ) at S370 (Fig. 4I, Supplementary Fig. S5B) was particularly intriguing since PKCθ activation by DAG is pivotal in modulating TCR signal strength and integrating TCR and co-stimulatory signals (39). Taken together, these findings showed that co-inhibition of both DGKα and DGKζ is required to effectively target T-cell DAG metabolism to improve TCR signaling, T-cell functionality and the combination benefit with PD-1 T-cell immune checkpoint therapy.

BMS-986408/anti-PD-1 combination therapy invigorates T-cell responses in NSCLC PDOTs

Next, we established the translational framework supporting the combination of PD-1 and DGKα/ζ inhibitors in NSCLC by, 1) establishing the expression of DGKα and DGKζ in T cells from NSCLC patient biopsies by scRNAseq and multiplex fluorescent immunohistochemistry, and 2) evaluating the benefit of both monotherapy and combination therapies in tumor-infiltrated lymphocytes (TILs) from freshly-resected NSCLC patient tumor tissue (Fig. 5A).

By revisiting public NSCLC scRNAseq datasets (26), we found *DGKA* and *DGKZ* were broadly expressed in TIL populations, including naïve T cells, $CD8^+$ effector memory T cells and NK cells (Fig. 5B). We observed that *DGKA* and *DGKZ* expression overlapped with T-cell exhaustion markers including *PDCD1* (PD-1), *TCF7* (TCF1; T cell factor 1) and *TOX* (TOX; thymocyte selection-associated high mobility group box) (40) (Fig. 5B). Next, DGKα and DGKζ protein expression was evaluated using multiplex immunofluorescence and digital pathology across 72 NSCLC patient tumor biopsies. DGKα and DGKζ were broadly expressed among $CD3^+CD4^+$ and $CD3^+CD8^+$ TILs (Fig. 5C and Supplementary Fig. S6A). Subpopulation analysis of exhausted T cells revealed that DGKα and/or DGKζ were expressed in both terminal (PD-1^+TOX^+) exhausted and progenitor (PD-1^+TCF1^+) exhausted $CD4^+$ and $CD8^+$ T cells (Fig. 5D). DGKα and DGKζ were more abundant compared to other co-inhibitor surface receptors CTLA-4, LAG3, TIGIT and TIM-3 (Fig. 5D). DGKα and DGKζ were also expressed in PD-1^- T cells (Fig. 5D). Taken together, these data show that DGKα and DGKζ are broadly expressed in NSCLC T cells and are therefore well positioned to negatively regulate both PD-1^+ and PD-1^- T cells.

As a first step toward establishing the translational relevance of our pre-clinical findings to the clinical setting we evaluated the combination of BMS-986408 and nivolumab (anti-PD-1) in NSCLC tumor specimens from treatment-naïve NSCLC patients (Patient metadata provided in Supplementary Table S5). Resected tumors were physically and enzymatically dissociated to generate fractions containing single cells (S3), Patient-Derived Organotypic Tumor spheroids (PDOTs; S2) (27), and tumor flakes (S1) (Supplementary Fig. S6B). Patient material included the tumor immune microenvironment, with immune content measured by the percentage of $CD45^+$ (immune) and $CD45^-$ (non-immune) cells within the S3 fraction (Supplementary Fig.

S6C and S6D). Highlighting the presence of immune infiltration into NSCLC and the potential patient impact of BMS-986408's effects in this setting, 10 of 11 clinical samples obtained showed evidence of high immune cell infiltration (Supplementary Fig. S6C). Clinical samples were treated with nivolumab, BMS-986408 or the combination for three days. Cytokine production was evaluated to indicate potential therapeutic response. T cells from baseline clinical samples expressed PD-1, and PD-1 expression increased in the majority of the patients following BMS-986408 monotherapy treatment (Supplementary Fig. S6E). Immune cell populations were comparable between treatment conditions at the end of three days (Supplementary Fig. S6D, S6F), indicating that changes in cytokine secretion were not due to proportional shifts in these populations. As a monotherapy, BMS-986408 induced more overall cytokine production than nivolumab, whereas the combination of BMS-986408 and nivolumab induced greater cytokine secretion than either monotherapy (Fig. 5E). We next focused on IFNγ, whose production is a hallmark of $CD8^+$ T-cell activation and cytotoxicity (41). While some patient samples showed response to nivolumab and/or BMS-986408 as single agents, combination treatment induced the greatest increases in IFNγ (Supplementary Fig. S6G). Combination treatment resulted in statistically significant increases in IFNγ in 6 of the 10 patient samples assessed (Pt. 2, 4, 8, 9, 10, and 11) compared to only 1 out of 10 (Pt. 8) for nivolumab and 1 out of 10 (Pt. 4) for BMS-986408 monotherapies (Fig. 5F). Tumor mutational burden (TMB) has been shown to be a predictive indicator of response to PD-1 inhibitors such as nivolumab (42). In patients deemed as IFNγ responders to the combination therapy, we observed significantly higher TMB than IFNγ non-responders (Fig. 5G). Taken together, these findings support the clinical evaluation of a dual DGKα/ζ inhibitor in combination with PD-1 T-cell immune checkpoint therapy in NSCLC patients.

DGKα/ζ inhibition unleashes CAR T-cell therapy

Next, we evaluated the therapeutic combination of BMS-986408 and CD19-directed CAR T-cell therapy. In a Raji B cell ($CD19^+$) tumor model, genetic knockout of *DGKA*, *DGKZ* or both in human CD19-targeting CAR T cells (Supplementary Fig. S7A) improved the depth and duration of tumor control with a rank order of *DGKA*/*DGKZ* > *DGKZ* > *DGKA* knockout (Fig. 6A and B, Supplementary Fig. S7B). CAR T-cell expansion in peripheral blood was modestly improved in the *DGKA* knockout (1.2× and 4.7× increase on days 12 and 19) and the *DGKZ* knockout (2.4× and 6.1× increase on days 12 and 19) CAR T cells (Fig. 6C), whereas there was a marked expansion with *DGKA*/*DGKZ* knockout (39.4× and 62.4× increase on days 12 and 19) (Fig. 6C). Co-dosing of BMS-986408 with wild type CAR T cells phenocopied both the improved tumor control and CAR T-cell expansion observed with the dual *DGKA*/*DGKZ* knockout (Fig. 6A-C; Supplementary Fig. S7B). This showed for that pharmacological inhibition of DGKα and DGKζ recapitulated the benefits observed with genetic knockout of *DGKA/DGKZ* in the CAR T-cell therapy setting.

Next, we explored how DGKα/ζ inhibition might overcome the loss of CAR T-cell functionality in the context of chronic antigen stimulation (43). Human CD19-targeting CAR T cells were subjected to chronic anti-idiotypic stimulation to induce a hypofunctional state (Supplementary Fig. S7C). As a result, these CAR T cells exhibited limited capacity to control the growth of either A549.CD19 or Granta-519 tumors in a 3D tumor co-culture (Fig. 6D and E). Addition of BMS-986408 elicited a robust, potent and dose-dependent decrease in A549.CD19 and Granta-519 tumor volume (Fig. 6D and E) and a corresponding increase in secretion of IFNγ, IL-2, and TNFα effector cytokines (Supplementary Fig. S7D). These findings showed that

dual DGKα/ζ inhibition can improve CAR T-cell therapy by overcoming chronic antigen stimulation induced hypo-functionality.

Next, we explored how DGKα/ζ inhibition might overcome a lack of CAR T-cell expansion elicited from inadequate T-cell costimulation. In contrast to Raji, K562 and Granta-519 cells that constitutively express costimulatory ligands, Nalm6 pre-B-cell acute lymphoblastic leukemia cells lack major costimulatory molecules such as CD80, CD86, CD40 or 41BB (Supplementary Fig. S7E). In this model, a sub-optimal dose of CD19-targeting CAR T cells (1×10^6 cells) slowed but did not eliminate tumor growth (Fig. 6F and G). BMS-986408 alone without CAR T cells was not efficacious as expected, while the combination of CAR T cells and BMS-986408 showed robust and durable tumor control (Fig. 6F and G; Supplementary Fig. S7F). Phenotyping of the peripheral blood showed that BMS-986408 markedly increased CAR T-cell expansion (Fig. 6H). Taken together, these findings suggest that dual DGKα/ζ inhibition may improve CAR T-cell activity in patients with difficult-to-treat tumors where CAR T cells are functionally impaired due to chronic antigen stimulation or lack of co-stimulation.

Discussion

BMS-986408 represents an advancement in the field of immunotherapy as a potent, first-in-class dual DGKα/ζ inhibitor, with the potential to broadly amplify T cell–mediated tumor immunity and invigorate both PD-1 immune checkpoint and CAR T-cell therapy. BMS-986408 is a potent DGKα and DGKζ lipid kinase inhibitor with a complex mechanism of action that includes binding to the accessory subdomain of the C-terminal catalytic domain, DAG-substrate competitive inhibition, subcellular translocation of DGKα/ζ to the plasma membrane, and proteosome-mediated degradation of DGKα/ζ. Identification of the BMS-986408 binding site

presented a substantial challenge as there are currently no solved structures for full-length proteins or the catalytic domains of mammalian DGKα or DGKζ by NMR, X-ray crystallography, or cryo-EM (31). As an alternative approach, we designed a CRISPR base editing strategy (32) that identified BMS-986408 resistance mutations clustered within the accessory subdomain of both DGKα and DGKζ. The findings that BMS-986408 binds within the accessory subdomain of the catalytic domain, is a DAG-substate competitive inhibitor, and mimics DAG-induced subcellular trafficking of DGKα and DGKζ to plasma membrane (44-46) suggest that the accessory subdomain harbors a DAG binding site(s) and BMS-986408 may act as a DAG mimic. To date, the DAG binding site(s) for mammalian DGKα and DGKζ has remained elusive. DAG-binding proteins (e.g., PKCs) bind to DAG through a typical C1 domain (47,48); however, DGKα and DGKζ have atypical C1 domains that do not directly bind to DAG but rather influence DAG fatty acyl specificity (49,50). The putative BMS-986408 binding pocket overlapped with the DAG and sphingosine binding sites for *Staphylococcus aureus* DgkB and Sphingosine kinase 1, respectively, which are two related lipid kinases with solved structures (34). Further efforts to structurally enable DGKα and/or DGKζ will be required to confirm that BMS-986408 and DAG share the same binding pockets. The discovery that BMS-986408 also induces proteosome-dependent degradation of both DGKα and DGKζ adds to a growing list of enzymatic inhibitors that also function as target protein degraders (51). Further efforts will be required to understand if BMS-986408 functions as a molecular glue recruiting an E3 ligase to DGKα and DGKζ or if perhaps the natural turnover of these proteins is accelerated due to conformational and/or subcellular localization changes.

PD-1 inhibitors have revolutionized the treatment landscape for NSCLC (52,53), but next-generation strategies are needed to improve overall response rate and durability. Our studies

have provided the pre-clinical and translational research framework to support the clinical evaluation of BMS-986408 and PD-1 T-cell immune checkpoint combination therapy in NSCLC and other indications where immune checkpoint inhibitors are approved (54). BMS-986408 markedly improved PD-1 inhibitor's therapeutic benefit in syngeneic mouse tumor models. BMS-986408 and anti-PD-1 synergized to amplify T-cell responses in the tumor while BMS-986408 also provided the unique benefit of amplifying tumor-reactive T-cell priming and expansion in TdLNs. Recent clinical data indicates that eliciting a polyclonal T-cell response is critical to drive productive antitumor immunity (55). The ability of BMS-986408 to amplify the priming and expansion of both high and low affinity TCR clonotypes provided compelling evidence that BMS-986408 could elicit a broader repertoire of tumor-reactive T cells to improve PD-1 therapy response. To begin translating these pre-clinical findings to patients, we evaluated DGKα/ζ expression in NSCLC patient biopsies. DGKα and DGKζ were broadly expressed in TILs, including both PD-1^+ and PD-1^- T cells, showing that DGKα and DGKζ are positioned to broadly regulate TILs. The breadth of their expression superseded well-established immune checkpoints such as CTLA-4, TIGIT and TIM-3 (56-58), suggesting that targeting DGKα/ζ could have broader impact. Further dissection of DGKα/ζ expression in TIL subsets revealed their enrichment in $TCF1^+$ progenitor exhausted and TOX^+ terminally exhausted T cells. The expression in progenitor exhausted T cells was of particular interest since this subset was found to be the major source of expanded tumor-reactive T cells in response to PD-1 therapy (59,60). Using NSCLC PDOTs (27,28), we showed that BMS-986408/nivolumab combination therapy improved both the depth and breadth of T-cell cytokine responses compared to either monotherapy. Moreover, combination therapy increased IFNγ production, whose production is a hallmark of $CD8^+$ T-cell activation and cytotoxicity (41). In responding tumors, we also

observed a significantly higher TMB, which correlates with more neoantigens and has been implicated as a predictive indicator of response to PD-1 inhibitors (42). These findings suggest that BMS-986408 could improve PD-1 therapy response by invigorating the functionality of tumor-reactive T cells while also expanding the repertoire of T-cell clonotypes and antigen specificities against a tumor.

Several other drug discovery efforts are underway to develop DGKα and DGKζ selective inhibitors (61,62). However, previous genetic studies showed that DGKα and DGKζ both regulate T-cell activation and effector functions (6,9). DGKζ appears to be the more dominant isozyme in regulating T-cell activation and antitumor immunity (11); however, DGKα upregulation has been implicated as a resistance mechanism to PD-1 therapy (5). Using mono-selective and dual pharmacological inhibitors, we showed that inhibiting both DGKα and DGKζ was required to maximize therapeutic benefit in combination with PD-1 therapy. Dual inhibition with BMS-986408 delivered equivalent efficacy to the combination of mono-selective inhibitors. This finding confirmed that a single dual inhibitor can achieve the same outcome as a combination approach with mono-selective inhibitors which offers a simpler path forward in the clinic. Using cellular assays, we showed that a dual inhibitor was superior to mono-selective inhibitors at improving T cell–mediated tumor killing and T-cell priming. The superiority of dual inhibitor was particularly evident for the priming and expansion of tumor-reactive T cells *in vivo*. Consistent with these findings, DGK inhibitor synergy studies and phospho-proteomics revealed that co-inhibition of DGKα and DGKζ was required to maximize TCR signaling downstream of DAG. Taken together, these findings strongly suggest that a dual DGKα/ζ targeting strategy will be necessary to fully realize the combination benefit potential with PD-1 therapy in the clinic.

CAR T-cell therapy is a cutting-edge treatment where a patient's own T cells are genetically engineered to recognize and destroy cancer cells (52,53). CD19-targeting (e.g., Breyanzi) and BCMA-targeting (e.g., Abecma) CAR T-cell therapies have been approved for hematological malignancies and many other CAR T-cell therapies are under clinical investigation across a variety of solid tumor indications (59,60). However, a large proportion of patients treated with CAR T cells relapse after an initial response. Lack of CAR T-cell persistence and diminished CAR T-cell function have been shown to contribute to the relapse (63). Based on genetic studies, deleting either *DGKA* and/or *DGKZ* has been proposed as a strategy to enhance CAR T-cell activity, improve their persistence, and increase their antitumor efficacy (6). We found that BMS-986408 phenocopied the therapeutic benefit of a dual *DGKA/DGKZ* genetic knockout showing that an inhibitor strategy is a feasible alternative to genetic engineering. Moreover, BMS-986408 overcame many of the hallmarks of poor CAR T-cell therapy response, including CAR T-cell hypofunctionality induced by chronic antigen stimulation, poor CAR T-cell expansion, and the absence of co-stimulatory ligands on target cells. The observation that DGKα/ζ inhibition improved CAR T-cell therapy in the absence of co-stimulatory ligands is of particular importance. CAR T-cell therapies for hematologic cancers benefit from ample costimulatory ligand engagement which helps to drive expansion and an efficacious antitumor response. Whereas in solid tumor setting, costimulation ligand expression is rare (64,65). These findings support the clinical evaluation of BMS-986408 with CAR T-cell therapy.

While these studies have focused on BMS-986408 combination with PD-1 immune checkpoint therapy and CAR T-cell therapy, the broad impact of DGKα/ζ inhibition on T-cell immunity warrants further investigation with other T-cell immune checkpoint therapies, cancer

vaccines, adoptive T-cell therapies and T-cell engagers. Taken together, BMS-986408 represents the first critical step towards evaluating the broad immunotherapy potential of DGKα/ζ inhibitors in cancer patients and the safety and tolerability of BMS-986408 alone and in combination with nivolumab is currently under clinical investigation (Clinicaltrials.gov ID: NCT05407675).

Acknowledgements

We are grateful to Bruce Ellsworth for critically reviewing the manuscript.

Author contributions

Michael Wichroski, Si-Qi Liu, Lauren M Zasadil, Patrick C. Gedeon, Kendall J. Condon, Suhasini Joshi, Shana Posy, Patrick Carlson, Alison Maier, and Joseph Benci were involved in the conceptualization, investigations, and authoring of the manuscript. Rakeeb Kureshi, Yuka Amako, Tai Wang, Ryan L. Powles, Yanyun Li, Tho Lai, Igor Katsyv, Hongchen Qiu, Huilin Qi, Jessica Wong, Dandan Zhao, Jon C. Jones, Dana Banas, Joelle Onorato, Gregory Locke, Xueer Chen, Wen-Chi Chou, Abigail E. Witt, Christopher M. Barbieri, Hong Zhang, Jonathan B. Olsen, Alba Font Tello, Eugene Drokhlyansky, John Wain, Denise C. Grünenfelder, Louis Chupak, and Tyler A. Longmire contributed to the investigations in the manuscript. Travis J. Hollmann, David G. Kugler, John N Feder, Raphael Bueno, Pallavur Sivakumar, Yu Liu, Stephanie K. Dougan, Cloud P. Paweletz, David A. Barbie, and Emma Lees provided supervision for the studies.

References

1. Waldman AD, Fritz JM, Lenardo MJ. A guide to cancer immunotherapy: from T cell basic science to clinical practice. Nat Rev Immunol **2020**;20(11):651-68 doi 10.1038/s41577-020-0306-5.
2. Sharma P, Hu-Lieskovan S, Wargo JA, Ribas A. Primary, Adaptive, and Acquired Resistance to Cancer Immunotherapy. Cell **2017**;168(4):707-23 doi 10.1016/j.cell.2017.01.017.
3. Wichroski M, Benci J, Liu SQ, Chupak L, Fang J, Cao C*, et al.* DGKalpha/zeta inhibitors combine with PD-1 checkpoint therapy to promote T cell-mediated antitumor immunity. Sci Transl Med **2023**;15(719):eadh1892 doi 10.1126/scitranslmed.adh1892.
4. Kureshi R, Bello E, Kureshi CTS, Walsh MJ, Lippert V, Hoffman MT*, et al.* DGKalpha/zeta inhibition lowers the TCR affinity threshold and potentiates antitumor immunity. Sci Adv **2023**;9(47):eadk1853 doi 10.1126/sciadv.adk1853.
5. Fu L, Li S, Xiao W, Yu K, Li S, Yuan S*, et al.* DGKA Mediates Resistance to PD-1 Blockade. Cancer Immunol Res **2021**;9(4):371-85 doi 10.1158/2326-6066.CIR-20-0216.
6. Jung IY, Kim YY, Yu HS, Lee M, Kim S, Lee J. CRISPR/Cas9-Mediated Knockout of DGK Improves Antitumor Activities of Human T Cells. Cancer Res **2018**;78(16):4692-703 doi 10.1158/0008-5472.CAN-18-0030.
7. Zhong XP, Guo R, Zhou H, Liu C, Wan CK. Diacylglycerol kinases in immune cell function and self-tolerance. Immunol Rev **2008**;224:249-64 doi 10.1111/j.1600-065X.2008.00647.x.
8. Krishna S, Zhong X. Role of diacylglycerol kinases in T cell development and function. Crit Rev Immunol **2013**;33(2):97-118 doi 10.1615/critrevimmunol.2013006696.
9. Guo R, Wan CK, Carpenter JH, Mousallem T, Boustany RM, Kuan CT*, et al.* Synergistic control of T cell development and tumor suppression by diacylglycerol kinase alpha and zeta. Proc Natl Acad Sci U S A **2008**;105(33):11909-14 doi 10.1073/pnas.0711856105.
10. Olenchock BA, Guo R, Carpenter JH, Jordan M, Topham MK, Koretzky GA*, et al.* Disruption of diacylglycerol metabolism impairs the induction of T cell anergy. Nat Immunol **2006**;7(11):1174-81 doi 10.1038/ni1400.
11. Gu J, Wang C, Cao C, Huang J, Holzhauer S, Desilva H*, et al.* DGKzeta exerts greater control than DGKalpha over CD8(+) T cell activity and tumor inhibition. Oncoimmunology **2021**;10(1):1941566 doi 10.1080/2162402X.2021.1941566.
12. Chupak L, Wichroski M, Zheng X, Ding M, Martin S, Allard C*, et al.* Discovery of Potent, Dual-Inhibitors of Diacylglycerol Kinases Alpha and Zeta Guided by Phenotypic Optimization. ACS Med Chem Lett **2023**;14(7):929-35 doi 10.1021/acsmedchemlett.3c00063.
13. Wang X, Tilford C, Neuhaus I, Mintier G, Guo Q, Feder JN*, et al.* CRISPR-DAV: CRISPR NGS data analysis and visualization pipeline. Bioinformatics **2017**;33(23):3811-2 doi 10.1093/bioinformatics/btx518.
14. Hanna RE, Hegde M, Fagre CR, DeWeirdt PC, Sangree AK, Szegletes Z*, et al.* Massively parallel assessment of human variants with base editor screens. Cell **2021**;184(4):1064-80 e20 doi 10.1016/j.cell.2021.01.012.
15. Martinez NJ, Asawa RR, Cyr MG, Zakharov A, Urban DJ, Roth JS*, et al.* A widely-applicable high-throughput cellular thermal shift assay (CETSA) using split Nano Luciferase. Sci Rep **2018**;8(1):9472 doi 10.1038/s41598-018-27834-y.
16. Dobin A, Davis CA, Schlesinger F, Drenkow J, Zaleski C, Jha S*, et al.* STAR: ultrafast universal RNA-seq aligner. Bioinformatics **2013**;29(1):15-21 doi 10.1093/bioinformatics/bts635.
17. Li B, Dewey CN. RSEM: accurate transcript quantification from RNA-Seq data with or without a reference genome. BMC Bioinformatics **2011**;12:323 doi 10.1186/1471-2105-12-323.

18. Ritchie ME, Phipson B, Wu D, Hu Y, Law CW, Shi W*, et al.* limma powers differential expression analyses for RNA-sequencing and microarray studies. Nucleic Acids Res **2015**;43(7):e47 doi 10.1093/nar/gkv007.
19. Law CW, Chen Y, Shi W, Smyth GK. voom: Precision weights unlock linear model analysis tools for RNA-seq read counts. Genome Biol **2014**;15(2):R29 doi 10.1186/gb-2014-15-2-r29.
20. Robinson MD, McCarthy DJ, Smyth GK. edgeR: a Bioconductor package for differential expression analysis of digital gene expression data. Bioinformatics **2010**;26(1):139-40 doi 10.1093/bioinformatics/btp616.
21. Clancy-Thompson E, Devlin CA, Tyler PM, Servos MM, Ali LR, Ventre KS*, et al.* Altered Binding of Tumor Antigenic Peptides to MHC Class I Affects CD8(+) T Cell-Effector Responses. Cancer Immunol Res **2018**;6(12):1524-36 doi 10.1158/2326-6066.CIR-18-0348.
22. Dougan SK, Dougan M, Kim J, Turner JA, Ogata S, Cho HI*, et al.* Transnuclear TRP1-specific CD8 T cells with high or low affinity TCRs show equivalent antitumor activity. Cancer Immunol Res **2013**;1(2):99-111 doi 10.1158/2326-6066.CIR-13-0047.
23. Ianevski A, Giri AK, Aittokallio T. SynergyFinder 3.0: an interactive analysis and consensus interpretation of multi-drug synergies across multiple samples. Nucleic Acids Res **2022**;50(W1):W739-W43 doi 10.1093/nar/gkac382.
24. Demichev V, Messner CB, Vernardis SI, Lilley KS, Ralser M. DIA-NN: neural networks and interference correction enable deep proteome coverage in high throughput. Nat Methods **2020**;17(1):41-4 doi 10.1038/s41592-019-0638-x.
25. Ritz C, Baty F, Streibig JC, Gerhard D. Dose-Response Analysis Using R. PLoS One **2015**;10(12):e0146021 doi 10.1371/journal.pone.0146021.
26. Prazanowska KH, Lim SB. An integrated single-cell transcriptomic dataset for non-small cell lung cancer. Sci Data **2023**;10(1):167 doi 10.1038/s41597-023-02074-6.
27. Jenkins RW, Aref AR, Lizotte PH, Ivanova E, Stinson S, Zhou CW*, et al.* Ex Vivo Profiling of PD-1 Blockade Using Organotypic Tumor Spheroids. Cancer Discov **2018**;8(2):196-215 doi 10.1158/2159-8290.CD-17-0833.
28. Aref AR, Campisi M, Ivanova E, Portell A, Larios D, Piel BP*, et al.* 3D microfluidic ex vivo culture of organotypic tumor spheroids to model immune checkpoint blockade. Lab Chip **2018**;18(20):3129-43 doi 10.1039/c8lc00322j.
29. Corwin WL, Ebrahimi-Nik H, Floyd SM, Tavousi P, Mandoiu, II, Srivastava PK. Tumor Control Index as a new tool to assess tumor growth in experimental animals. J Immunol Methods **2017**;445:71-6 doi 10.1016/j.jim.2017.03.013.
30. Franks CE, Campbell ST, Purow BW, Harris TE, Hsu KL. The Ligand Binding Landscape of Diacylglycerol Kinases. Cell Chem Biol **2017**;24(7):870-80 e5 doi 10.1016/j.chembiol.2017.06.007.
31. Ma Q, Srinivasan L, Gabelli SB, Raben DM. Elusive structure of mammalian DGKs. Adv Biol Regul **2022**;83:100847 doi 10.1016/j.jbior.2021.100847.
32. Komor AC, Kim YB, Packer MS, Zuris JA, Liu DR. Programmable editing of a target base in genomic DNA without double-stranded DNA cleavage. Nature **2016**;533(7603):420-4 doi 10.1038/nature17946.
33. Friesner RA, Banks JL, Murphy RB, Halgren TA, Klicic JJ, Mainz DT*, et al.* Glide: a new approach for rapid, accurate docking and scoring. 1. Method and assessment of docking accuracy. J Med Chem **2004**;47(7):1739-49 doi 10.1021/jm0306430.
34. Ma Q, Gabelli SB, Raben DM. Diacylglycerol kinases: Relationship to other lipid kinases. Adv Biol Regul **2019**;71:104-10 doi 10.1016/j.jbior.2018.09.014.
35. Ashouri JF, Weiss A. Endogenous Nur77 Is a Specific Indicator of Antigen Receptor Signaling in Human T and B Cells. J Immunol **2017**;198(2):657-68 doi 10.4049/jimmunol.1601301.

36. Berenbaum MC. What is synergy? Pharmacol Rev **1989**;41(2):93-141.
37. Zhong XP, Hainey EA, Olenchock BA, Zhao H, Topham MK, Koretzky GA. Regulation of T cell receptor-induced activation of the Ras-ERK pathway by diacylglycerol kinase zeta. J Biol Chem **2002**;277(34):31089-98 doi 10.1074/jbc.M203818200.
38. Navarro MN, Feijoo-Carnero C, Arandilla AG, Trost M, Cantrell DA. Protein kinase D2 is a digital amplifier of T cell receptor-stimulated diacylglycerol signaling in naive CD8(+) T cells. Sci Signal **2014**;7(348):ra99 doi 10.1126/scisignal.2005477.
39. Isakov N, Altman A. Protein kinase Cθ in T cell activation. Annual Review of Immunology **2002**;20:761-94 doi DOI 10.1146/annurev.immunol.20.100301.064807.
40. Kallies A, Zehn D, Utzschneider DT. Precursor exhausted T cells: key to successful immunotherapy? Nat Rev Immunol **2020**;20(2):128-36 doi 10.1038/s41577-019-0223-7.
41. Bhat P, Leggatt G, Waterhouse N, Frazer IH. Interferon-gamma derived from cytotoxic lymphocytes directly enhances their motility and cytotoxicity. Cell Death Dis **2017**;8(6):e2836 doi 10.1038/cddis.2017.67.
42. Greillier L, Tomasini P, Barlesi F. The clinical utility of tumor mutational burden in non-small cell lung cancer. Transl Lung Cancer Res **2018**;7(6):639-46 doi 10.21037/tlcr.2018.10.08.
43. Liu C, Qi T, Milner JJ, Lu Y, Cao Y. Speed and Location Both Matter: Antigen Stimulus Dynamics Controls CAR-T Cell Response. Front Immunol **2021**;12:748768 doi 10.3389/fimmu.2021.748768.
44. Santos T, Carrasco S, Jones DR, Merida I, Eguinoa A. Dynamics of diacylglycerol kinase zeta translocation in living T-cells. Study of the structural domain requirements for translocation and activity. J Biol Chem **2002**;277(33):30300-9 doi 10.1074/jbc.M200999200.
45. Merino E, Avila-Flores A, Shirai Y, Moraga I, Saito N, Merida I. Lck-dependent tyrosine phosphorylation of diacylglycerol kinase alpha regulates its membrane association in T cells. J Immunol **2008**;180(9):5805-15 doi 10.4049/jimmunol.180.9.5805.
46. Baldanzi G, Cutrupi S, Chianale F, Gnocchi V, Rainero E, Porporato P*, et al.* Diacylglycerol kinase-alpha phosphorylation by Src on Y335 is required for activation, membrane recruitment and Hgf-induced cell motility. Oncogene **2008**;27(7):942-56 doi 10.1038/sj.onc.1210717.
47. Colon-Gonzalez F, Kazanietz MG. C1 domains exposed: from diacylglycerol binding to protein-protein interactions. Biochim Biophys Acta **2006**;1761(8):827-37 doi 10.1016/j.bbalip.2006.05.001.
48. Katti SS, Krieger IV, Ann J, Lee J, Sacchettini JC, Igumenova TI. Structural anatomy of Protein Kinase C C1 domain interactions with diacylglycerol and other agonists. Nat Commun **2022**;13(1):2695 doi 10.1038/s41467-022-30389-2.
49. Ware TB, Franks CE, Granade ME, Zhang M, Kim KB, Park KS*, et al.* Reprogramming fatty acyl specificity of lipid kinases via C1 domain engineering. Nat Chem Biol **2020**;16(2):170-8 doi 10.1038/s41589-019-0445-9.
50. Hurley JH, Misra S. Signaling and subcellular targeting by membrane-binding domains. Annu Rev Biophys Biomol Struct **2000**;29:49-79 doi 10.1146/annurev.biophys.29.1.49.
51. Kozicka Z, Thoma NH. Haven't got a glue: Protein surface variation for the design of molecular glue degraders. Cell Chem Biol **2021**;28(7):1032-47 doi 10.1016/j.chembiol.2021.04.009.
52. Garon EB, Rizvi NA, Hui R, Leighl N, Balmanoukian AS, Eder JP*, et al.* Pembrolizumab for the treatment of non-small-cell lung cancer. N Engl J Med **2015**;372(21):2018-28 doi 10.1056/NEJMoa1501824.
53. Gettinger S, Rizvi NA, Chow LQ, Borghaei H, Brahmer J, Ready N*, et al.* Nivolumab Monotherapy for First-Line Treatment of Advanced Non-Small-Cell Lung Cancer. J Clin Oncol **2016**;34(25):2980-7 doi 10.1200/JCO.2016.66.9929.

54. Sharma P, Goswami S, Raychaudhuri D, Siddiqui BA, Singh P, Nagarajan A*, et al.* Immune checkpoint therapy-current perspectives and future directions. Cell **2023**;186(8):1652-69 doi 10.1016/j.cell.2023.03.006.
55. Valpione S, Mundra PA, Galvani E, Campana LG, Lorigan P, De Rosa F*, et al.* The T cell receptor repertoire of tumor infiltrating T cells is predictive and prognostic for cancer survival. Nat Commun **2021**;12(1):4098 doi 10.1038/s41467-021-24343-x.
56. Cho BC, Abreu DR, Hussein M, Cobo M, Patel AJ, Secen N*, et al.* Tiragolumab plus atezolizumab versus placebo plus atezolizumab as a first-line treatment for PD-L1-selected non-small-cell lung cancer (CITYSCAPE): primary and follow-up analyses of a randomised, double-blind, phase 2 study. Lancet Oncol **2022**;23(6):781-92 doi 10.1016/S1470-2045(22)00226-1.
57. Curigliano G, Gelderblom H, Mach N, Doi T, Tai D, Forde PM*, et al.* Phase I/Ib Clinical Trial of Sabatolimab, an Anti-TIM-3 Antibody, Alone and in Combination with Spartalizumab, an Anti-PD-1 Antibody, in Advanced Solid Tumors. Clin Cancer Res **2021**;27(13):3620-9 doi 10.1158/1078-0432.CCR-20-4746.
58. Hodi FS, O'Day SJ, McDermott DF, Weber RW, Sosman JA, Haanen JB*, et al.* Improved survival with ipilimumab in patients with metastatic melanoma. N Engl J Med **2010**;363(8):711-23 doi 10.1056/NEJMoa1003466.
59. Gill AL, Wang PH, Lee J, Hudson WH, Ando S, Araki K*, et al.* PD-1 blockade increases the self-renewal of stem-like CD8 T cells to compensate for their accelerated differentiation into effectors. Sci Immunol **2023**;8(86):eadg0539 doi 10.1126/sciimmunol.adg0539.
60. Lee J, Ahn E, Kissick HT, Ahmed R. Reinvigorating Exhausted T Cells by Blockade of the PD-1 Pathway. For Immunopathol Dis Therap **2015**;6(1-2):7-17 doi 10.1615/ForumImmunDisTher.2015014188.
61. Patel MR, Park DJ, Tarantolo S, Dowlati A, Olson D, Kaneko Y*, et al.* Abstract CT132: Trial in progress: A phase 1/2 study of ASP1570, a novel inhibitor of DGKζ, in participants with locally advanced or metastatic solid tumors who have progressed on, or are ineligible for, all available standard therapies. Cancer Research **2023**;83(8_Supplement):CT132-CT doi 10.1158/1538-7445.Am2023-ct132.
62. Offringa R, Olesch C, Cichon F, Grees M, Schmees N, Roehn U*, et al.* Abstract ND04: BAY 2965501: A highly selective DGK- ζ inhibitor for cancer immuno-therapy with first-in-class potential. Cancer Research **2023**;83(7_Supplement):ND04-ND doi 10.1158/1538-7445.Am2023-nd04.
63. Singh AP, Chen W, Zheng X, Mody H, Carpenter TJ, Zong A*, et al.* Bench-to-bedside translation of chimeric antigen receptor (CAR) T cells using a multiscale systems pharmacokinetic-pharmacodynamic model: A case study with anti-BCMA CAR-T. CPT Pharmacometrics Syst Pharmacol **2021**;10(4):362-76 doi 10.1002/psp4.12598.
64. Harrison AJ, Du X, von Scheidt B, Kershaw MH, Slaney CY. Enhancing co-stimulation of CAR T cells to improve treatment outcomes in solid cancers. Immunother Adv **2021**;1(1):ltab016 doi 10.1093/immadv/ltab016.
65. Honikel MM, Olejniczak SH. Co-Stimulatory Receptor Signaling in CAR-T Cells. Biomolecules **2022**;12(9) doi 10.3390/biom12091303.

Figure Legends

Fig. 1. **BMS-986408 is a potent DGKα and DGKζ lipid kinase inhibitor and degrader**.

A, Chemical structure of BMS-986408. **B**, Plots showing the inhibitory dose response curves for BMS-986408 in recombinant DGKα and DGKζ biochemical lipid kinase assays and corresponding half-maximal inhibitory concentration (IC_{50}). **C**, Conversion of D4-Oloeyl-DAG to D4-Oleoyl PA in Jurkat cells treated with 0.25 μM of BMS-986408. Data are mean ± s.d.; n = 3 per group. **D**, Schematic of the BMS-986408 NanoBRET target engagement assay in live cells. Schematic was created with BioRender.com. **E**, Time lapse of mBRET ratio with the BMS-986408-NB590 tracer in DGKα-NanoLuc and NanoLuc-DGKζ overexpressing cells with (■) or without (●) saturating unlabeled BMS-986408 (20 μM) to normalize for specificity (top panels) and DGKi-NB590 binding kinetics to DGKα-NanoLuc and NanoLuc-DGKζ (bottom panels). Binding affinity is presented in K_d; Data are mean ± s.d.; n = 2 per group. **F**, CETSA melting curves of DGKα (top panel) and DGKζ (bottom panel) from Jurkat cells treated with (●) or without (●) 0.5 μM BMS-986408. Data shows the percent change from the 37°C baseline. **G**, Representative images showing the subcellular localization of YFP tagged DGKα or DGKζ with or without BMS-986408 (0.25 μM). YFP is colored in green and nuclear staining colored in blue. **H**, Quantification of BMS-986408 induced DGKα (●) and DGKζ (◆) plasma-membrane translocation with half-maximal efficacious concentrations (EC_{50}). **I**, Degradation dose-response for DGKα and DGKζ in human PBMCs treated with BMS-986408 for 24h. β-actin is presented as a loading control. **J**, Rescue of BMS-986408-mediated degradation with proteosome (Bortezomib, BZ) and ubiquitination (TAK-243, E1i) inhibitors. **K**, Schematic of the whole blood DGKi potency assay, highlighting phospho-ERK and IL-2 pharmacodynamic biomarkers. **L**, Flow cytometry quantification of BMS-986408 phospho-ERK induction potency in whole blood T cells. EC_{50} is shown for CD4+ (●) and CD8+ (●) T cells. Data are mean ± s.d.; n = 11 per group. **M**, AlphaLISA quantification of BMS-986408 IL-2 production from human whole blood from 2 donors. EC_{50} is shown for each donor.

Fig. 2. **BMS-986408 binds with the accessory region of DGKα and DGKζ lipid kinase domain.**

A, Schematic of the CRISPR base editing screen to select for *DGKA* or *DGKZ* mutations that conferred resistance to BMS-986408-mediated degradation of eGFP-DGKα or mNeonGreen-DGKζ expressed in Jurkat cells. Illustration was created with BioRender.com. **B** and **C**, Scatterplot of Log2 Fold Change (LFC) sgRNA enrichment in *DGKA* and *DGKZ* adenine base editor scanning screens. The dotted line indicates LFC=1.5 and validated hits are highlighted in green. AlphaFold models of DGKα and DGKζ are shown as ribbons with C-alpha atoms of enriched residues shown as spheres. The surfaces of the docked ligands (see Methods) are shown to highlight the proposed binding sites. **D**, Validation of the base editing CRISPR screen using knock-in cell clones: Jurkat eGFP-DGKα cells harboring the S532P, L556P or H606R mutations and mNeonGreen-DGKζ cells harboring the F463S, S490P, or C534R mutations were treated with BMS-986408 (0.75 μM) and fluorescence signal was quantified as mean fluorescence intensity (MFI). Each point represents a cell clone. **E**, BMS-986408 CETSA dose-response at 41.5°C showing that HiBit-tagged DGKα harboring the S532P, L556P or H606R mutations was

resistant to BMS-986408-mediated thermal destabilization. **F**, BMS-986408 CETSA dose-response at 43.1°C showing HiBit-tagged DGKζ harboring the F463S, S490P, or C534R mutations were resistant to BMS-986408-mediated thermal destabilization. **G,** Closer view of docked poses with enriched residues' side chains shown as orange sticks and validated residues' side chains shown as green sticks. **H**, Electrostatic surface representation of the proposed binding sites, with the surfaces of validated residues shown in green.

Fig. 3. **Dual DGKα/ζ inhibitor BMS-986408 unleashes PD-1 T cell checkpoint therapy.**

A, Schematic of TCR signaling cascade, with TCR and CD28 providing positive signals and PD-1 and DGKα/ζ providing negative signals. **B**, Therapeutic efficacy of anti-PD1, BMS-986408 or combination therapy in SA1N, MC38 and CT26 tumor models. Each line represents tumor volume of one individual animal. n=10 per group. The percentage of animals achieving complete tumor regression (CR) is noted on each plot. **C**, Heatmap of differentially expressed genes from RNAseq data from MC38 tumors at day 7 post treatment. The black and grey barcodes indicates whether the expression change is statistically different between the vehicle and combination treatment group. **D**, Volcano plots of RNAseq data from the same analysis. Upregulated genes are highlighted in purple and downregulated genes in blue; a subset of upregulated T cell effector genes are labeled in each plot. **E**, Flow cytometry quantification of Granzyme B+ and Ki67+ effector CD8+ populations in the MC38 tumors. Data was collected at day 7 post treatment initiation. **F**, Flow cytometry quantification of naïve (CD44- CD62L+), effector/effector memory (E/EM, CD44+ CD62L-), central memory (CM, CD44+ CD62L+) and activated (CD69+, PD-1+ or Ki67+) CD8+ T cell subsets in MC38 tumor-draining lymph nodes (TdLN). Data was collected at day 7 post treatment initiation. **G**, Flow cytometric quantification of GFP+ CD8+ T cells in the TdLN of MC38 tumors implanted into Nur77-GFP transgenic mice. Data was collected 24h after treatment with anti-PD-1, BMS-986408 or the combination. **H**, *In vivo* priming of tumor antigen-specific T cells. $TRP1^{high}$ or $TRP1^{low}$ transgenic CD8+ T cells were labeled with CTV and were adoptively transferred into mice implanted with C2VTrp1 tumors. Mice were dosed with anti-PD-1, BMS-986408 or combination treatment. Representative flow cytometry analysis of CTV dilution in adoptively transferred cells are shown. Gates delineate different generations of proliferated cells. **I**, Calculated proliferation index (see Methods) of adoptively transferred $TRP1^{High}$ and $TRP1^{Low}$ CD8+ T cells in the TdLN 5 days after treatment with either anti-PD-1, BMS-986408 or the combination; n=5 per group. Statistical analysis was performed using an ordinary one-way ANOVA, $*P < 0.05$ $**P < 0.01$, $***P < 0.001$, and $****P < 0.0001$. Error bars represent s.d.

Fig. 4. **Inhibiting both DGKα and DGKζ maximizes anti-PD-1 combination benefit.**

A, Therapeutic efficacy of anti-PD-1 versus the combination of anti-PD-1 with either BMS-986408, DGKα-i, DGKζ-i or DGKα-i + DGKζ-i in the MC38 tumor model. Each line represents the tumor volume curve from one individual animal. The percentage of animals achieving CR is noted on each plot. **B**, Cytotoxicity evaluation of NY-ESO-1 specific effector T cells in the presence of DGKα-i, DGKζ-i or BMS-408. All compounds were dosed at 0.1 μM; n=6 per group. **C**, Proliferation of human PBMC (left panel) and mouse $TRP1^{high}$ T cells (right panel) in the presence of DGKα-i, DGKζ-i or BMS-408. All compounds were dosed at 0.1 μM; n=5 per

group. **D**, *In vivo* proliferation indices of adoptively transferred TRP1^{high} T cells, in recipient mice dosed with DGKα-i, DGKζ-i, or BMS-408; n=5 per group. **E** and **F**, Human PBMC proliferation and IFNγ production in a matrixed combination dose-response of DGKα-i or DGKζ-i (left panel) with corresponding HSA synergy analysis (right panel); n=6 per group. **G**, Heatmap of phospho-peptides significantly changed in human T cells treated with dose titrations of DGKα-i, DGKζ-i, or BMS-986408 from 0.001μM to 1 μM. Values represent the signed effect size of the dose response curves (see Methods), with purple showing increased phosphorylation and blue showing decreased phosphorylation. **H**, KEGG pathway enrichment analysis of significantly increased phosphoproteins from **G**. Top 10 pathways with -$\log_{10}$[False Discovery Rate (FDR)] is presented. **I**, Dose effect sizes of selected phospho-peptides from the NFκB pathway and MAPK pathway as in **G**. Statistical analysis was performed using an ordinary one-way ANOVA, **P* < 0.05 ***P* < 0.01, ****P* < 0.001, and *****P* < 0.0001. Error bars represent s.d.

Fig. 5. **Translational data supporting the combination of DGKα/ζ and PD-1 inhibitors in NSCLC.**

A, Schematic of the translational research strategy to evaluate DGKα/ζ expression and inhibition in NSCLC patient tumor biopsies. Illustration was created with BioRender.com. **B**, Umap plot of scRNAseq data from NSCLC patients (see Methods). Immune cell populations were plotted and color-coded by their corresponding signature gene expression. Right panel shows the expression overlay of genes of interest. **C**, Representative multiplexed immunofluorescence (mIF) images showing the expression of CD3, CD4, CD8, PD1, DGKα and DGKζ in a NSCLC patient tumor biopsy. **D**, Dot plot summary of DGKα, DGKζ and several additional immune checkpoint expression in NSCLC TIL subsets from 78 NSCLC patients. Dot sizes represent $\log_2$ cell count and dot colors represent $\log_2$ mIF intensity. **E**, Cytokine quantification in the PDOT cultures with anti-PD-1, BMS-408, or combination treatment. **F**, Absolute quantification of IFNγ release in PDOT cultures, grouped by each individual patients, and further divided into Responders/Non-responders based on whether anti-PD-1 and BMS-408 combination induced significant increase of IFNγ release. Statistical analysis was performed using an ordinary one-way ANOVA, **P* < 0.05 ***P* < 0.01, ****P* < 0.001, and *****P* < 0.001. Error bars represent s.d. **G**, Tumor mutation burden of PDOT tumors grouped by IFNγ Responder status. Student *t*-test was performed between the two groups. ***P* < 0.01. In all studies, data were collected 3 days after treatment, and BMS-986408 was dosed at 0.3 μM.

Fig. 6. **Dual DGKα/ζ inhibitor BMS-986408 unleashes CAR-T cell therapy.**

A, Growth curves of Raji transduced with red-shifted firefly luciferase (Raji-rFluc) tumor in NSG mice over time. Mice were given a suboptimal dose of 1×10^6 CAR-T cells of different genotypes and dosed with or without 0.3 mpk BMS-986408. **B** and **C**, Modified tumor control index (see Methods) and CAR-T cells per μL blood from each group. Non-parametric Kruskal–Wallis test was performed followed by the Benjamini, Krieger and Yekutieli false-discovery rate (FDR) correction for multiple comparisons. **D** and **E**, Chronically stimulated CAR-T cells were removed from plate-bound stimulus and plated with A549.CD19 or Granta-519 3D spheroids with varying treatment levels of BMS-986408. Normalized tumor area (RCU μm2) was assessed

on day 9. Friedman test was performed with Dunn's post-test for multiple comparisons. *P<0.05, ** P <0.01. **F**, Growth curves of Nalm6 transduced with red-shifted firefly luciferase (Nalm6-rFluc) tumor in NSG mice over time. Mice were dosed with BMS-986408 (0.3 mpk), 1×10^6 CAR-T cells or combination of both. **G**, Nalm6-rFluc tumor growth curves were analyzed calculated as modified tumor control index. Student *t*-test was performed between the two groups, ****P<0.0001. **H**, Blood circulating CAR-T cells were quantified by flow cytometry on days 8, 16, 23, and 30. For all plots, error bars represent s.d.

Fig. 1

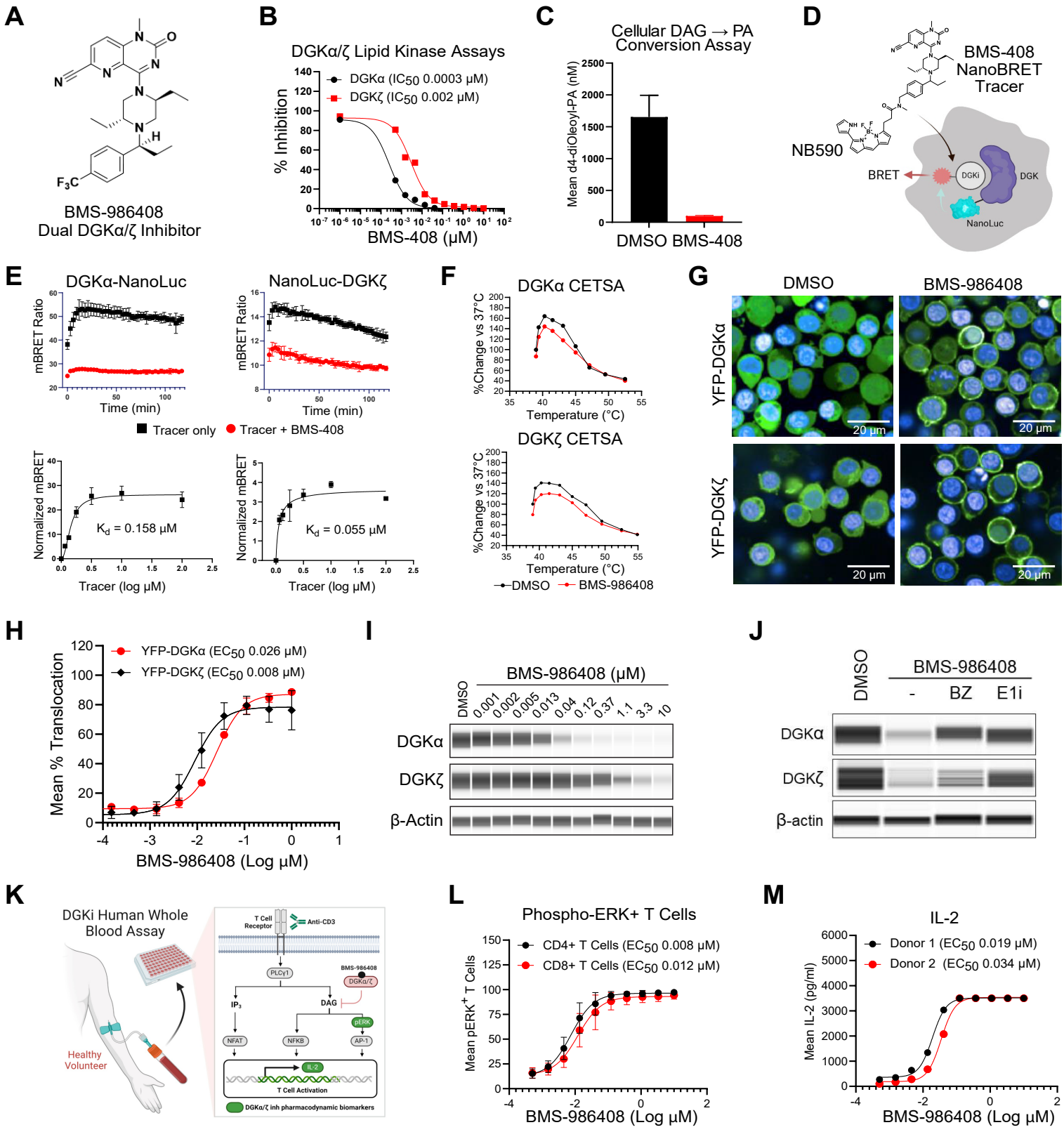

Fig. 2

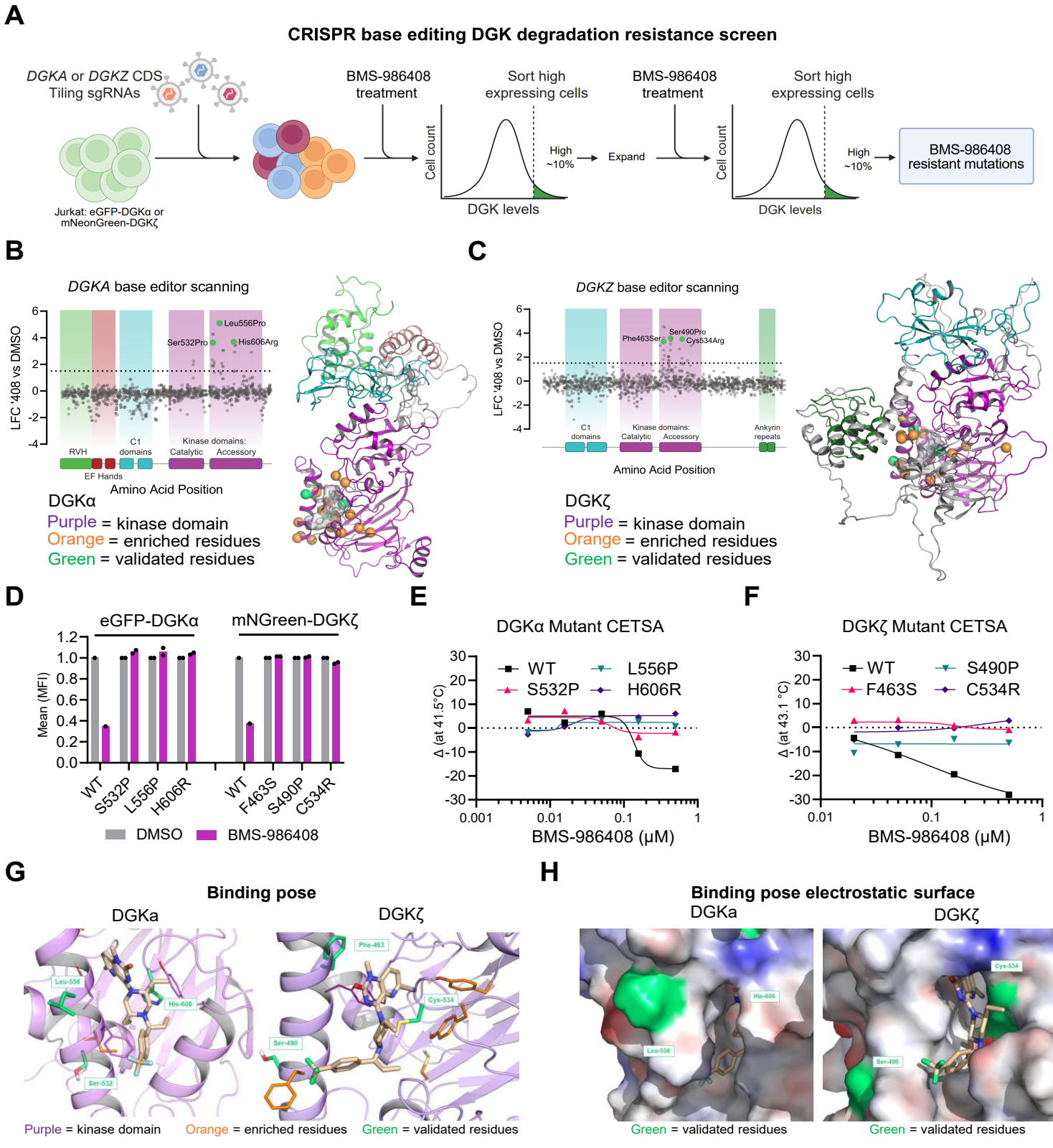

Fig. 3

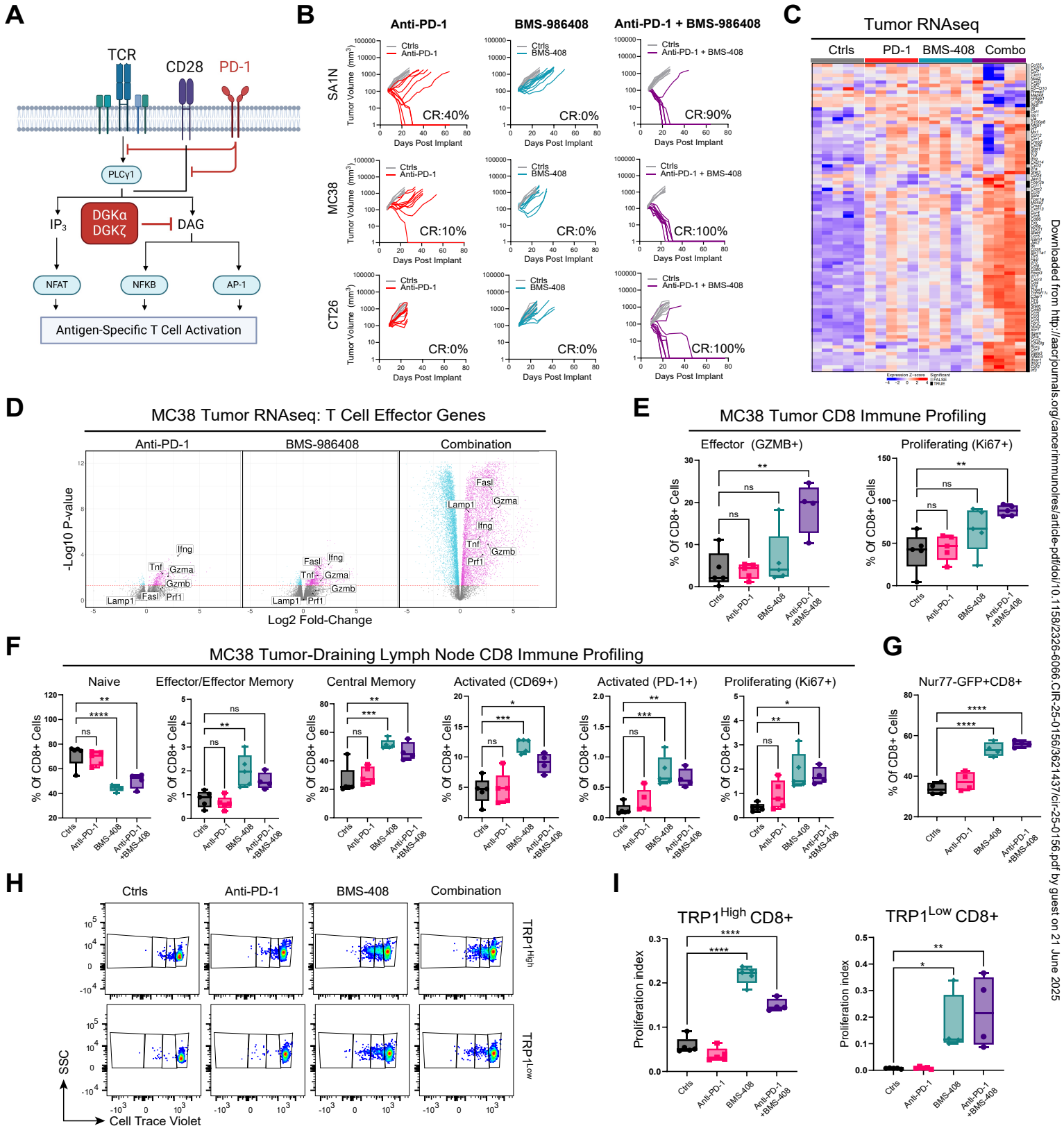

Fig. 4

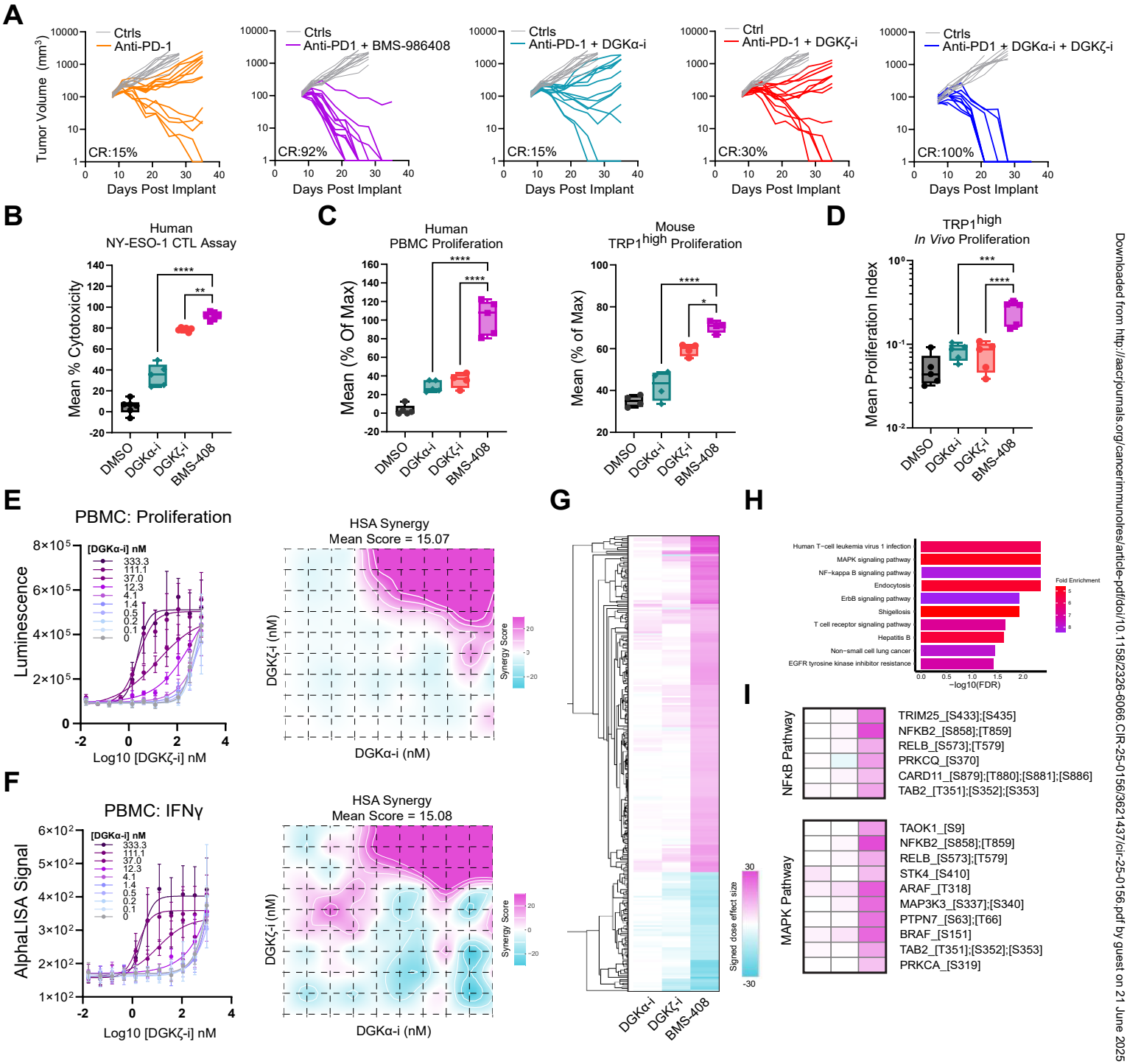

Fig. 5

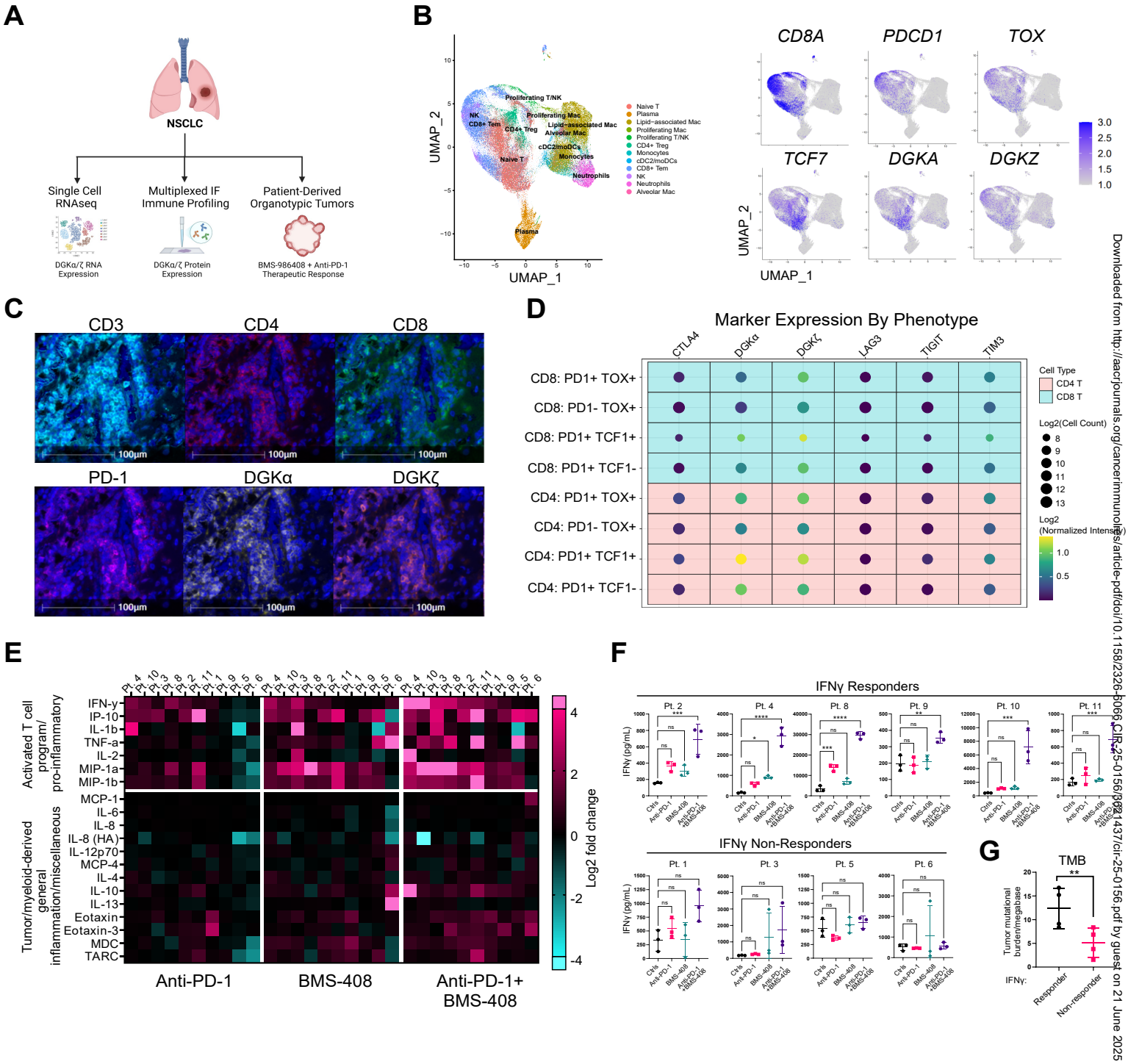

Fig. 6